

# Photoproduction of the Very Strangest Baryons on a Proton Target in CLAS12

A. Afanasev, W.J. Briscoe, H. Haberzettl, I.I. Strakovsky\*, and R.L. Workman

*The George Washington University, Washington, DC 20052, USA*

M.J. Amaryan, G. Gavalian, and M.C. Kunkel

*Old Dominion University, Norfolk, VA 23529, USA*

Ya.I. Azimov

*Petersburg Nuclear Physics Institute, Gatchina, Russia 188300*

N. Baltzell

*Argonne National Laboratory, Argonne, IL 60439, USA*

M. Battaglieri, A. Celentano, R. De Vita, M. Osipenko, M. Ripani, and M. Taiuti

*INFN, Sezione di Genova, 16146 Genova, Italy*

V.N. Baturin, S. Boyarinov, D.S. Carman, V. Kubarovsky,

V. Moiseev, E. Pasyuk\*, S. Stepanyan, D.P. Weygand, and V. Ziegler\*

*Thomas Jefferson National Accelerator Facility, Newport News, VA 23606, USA*

W. Boeglin, J. Bono, L. Guo\*,\*\*, P. Khetarpal, P. Markowitz, and B. Raue

*Florida International University, Miami, FL 33199, USA*

S. Capstick, V. Crede, and W. Roberts

*Florida State University, Tallahassee, FL 32306, USA*

M. Dugger\* and B.G. Ritchie

*Arizona State University, Tempe, AZ 85287-1504, USA*

G. Fedotov

*University of South Carolina, Columbia, SC 29208, USA*

J. Goetz\* and B.M.K. Nefkens

*University of California at Los Angeles, Los Angeles, CA 90095, USA*

D.I. Glazier and D.P. Watts\*

*Edinburgh University, Edinburgh EH9 3JZ, United Kingdom*

S. Hasegava, H. Sako, S. Sato, and K. Shirotori

*Japan Atomic Energy Agency, 2-4 Tokai-mura, Naka-gun, Ibaraki-ken 319-1195, Japan*

K. Hicks

*Ohio University, Athens, OH 45701, USA*

D.G. Ireland, K. Livingston, and B. McKinnon

*University of Glasgow, Glasgow G12 8QQ, United Kingdom*

F.J. Klein and N. Walford

*The Catholic University of America, Washington, DC 20064, USA*

A. Kubarovsky

*Rensselaer Polytechnic Institute, Troy, NY 12180-3590, USA*

H. Lu and P. Mattione

*Carnegie Mellon University, Pittsburgh, PA 15213, USA*

K. Nakayama

*University of Georgia, Athens, GA 30602, USA*

Yongseok Oh

*Kyungpook National University, Daegu 702-701, Republic of Korea*

M. Paolone

*Temple University, Philadelphia, PA 19122, USA*

J.W. Price

*California State University, Dominguez Hills, Carson, CA 90747, USA*

F. Sabatie

*CEA-Saclay, Service de Physique Nucléaire, 91191 Gif-sur-Yvette, France*

C. Salgado

*Norfolk State University, Norfolk, VA 23504, USA*

V. Shklyar

*Giessen University, D-35392 Giessen, Germany*

(The Very Strange Collaboration)

\*\* - Contact person, \* - Spokesperson

(Dated: May 3, 2012)

## Abstract

We propose to study the production mechanisms of the  $S = -2, -3$  baryons in exclusive photonuclear reactions with the CLAS12 detector.

The proposed experiment, to be run in parallel with the approved CLAS12 meson spectroscopy experiment [E12-11-005], is expected to yield total samples containing  $\sim 7000 \Omega^-$  ( $S = -3$ ) and several millions  $\Xi$  ( $S = -2$ ) baryons after reconstruction, based on predicted cross sections and simulated results.

These data would provide the statistics necessary to obtain the first precision measurement of the  $\Omega^-$  differential cross section in the reaction  $\gamma p \rightarrow \Omega^- K^+ K^+ K^0$ , and to search for excited  $\Omega^-$  states.

This experiment would provide the world's largest sample of cascade baryons in a photoproduction environment. Our cascade data sample would be used to search for new and missing excited  $\Xi$  states with the possibility to measure their quantum numbers, as well as the mass splittings of ground state and excited cascade doublets. In addition, we would extract spin-parity information of the already-established  $\Xi(1690)$  and  $\Xi(1820)$  from a double-moment analysis. These  $\Xi$  data samples would also provide the statistics necessary for measuring, for the first time as a function of kinematic variables, the beam polarization transfer and induced polarization of the ground state  $\Xi^-$  in the reaction  $\gamma p \rightarrow \Xi^- K^+ K^-$ .

## I. INTRODUCTION

Historically, baryons with multiple strange quarks have played an important role in the development of the quark model and our understanding of the universe. The prediction and discovery of the  $\Omega^-$  baryon certainly was one of the great triumphs of the quark model. However, half a century later, there has been little new information about the  $\Omega$  and  $\Xi$  baryons. In fact, only two  $\Omega$  states and six  $\Xi$  states are considered to be well-established, with at least three-star ratings in the PDG [1]. The production mechanism of these states is still unknown to a large extent. Typically small cross sections make the observation of the higher excited states difficult, which explains our current lack of knowledge in excited hyperon spectroscopy. Production of doubly- or triply-strange baryons by means of a photon beam (such as in the CLAS, at present, and CLAS12 and GlueX, in the future) is expected to shed light on the genesis of these states which involves the production of  $s\bar{s}$  pairs from the vacuum. This significant change in baryon strangeness number from initial ( $S = 0$ ) to final state ( $S = -3, -2$ ) could result from direct production via vector-meson dominance or from a sequence of intermediate transitions. Inference on the production mechanisms of these states in  $\gamma p$  collisions can be obtained from precision measurements of the cross section and invariant mass of these states.

Although the  $\Omega$  and  $\Xi$  baryons photoproduction rates are small, making the excited states difficult to observed with high significance, the expected narrowness of their widths would make it easier to identify and isolate them in the laboratory. For example, the  $\Xi$  excited states are typically 5 – 10 times narrower than their  $S = 0, -1$  counterparts. While many of the  $\Omega$  excited states remain unknown, it is natural to expect that they will exhibit similar features to those in the  $\Xi$  sector.

The 12 GeV Upgrade will provide an order of magnitude higher in luminosity and CLAS12 significantly better multiple-particle final states acceptance than CLAS. It is therefore expected that many aspects of  $\Omega^-$  and  $\Xi$  physics can be probed at CLAS12 using the quasi-real photon beams with the forward tagger.

The CLAS12 detector is expected to record sufficient statistics to perform several essential measurements to deepen our understanding of  $\Omega^-$  and  $\Xi$  states, including the cross section of the ground state  $\Omega^-$  and  $\Xi$  baryons, the mass splittings of of ground and excited cascades which would deepen our understanding of the  $u/d$  quark mass difference, and the polarization

of the  $\Xi^-$  baryon. The expected CLAS12 hyperon data samples would also provide spin-parity information for multiple excited cascades. Furthermore, the narrow width of cascades might be better understood from the experimental verification of decoupling of excited cascade from the  $\Xi\pi$  channel.

## II. PHYSICS MOTIVATION

### A. Search for the $\Omega$ -states in Photoproduction

The photoproduction of the ( $S = -3$ )  $\Omega$  baryon requires the a total strangeness transfer  $\Delta S = 3$ . This is the largest possible transfer of strangeness number, which makes the measurement of the production of this state and of its decay properties particularly interesting in a photoproduction environment, which have not yet been established.

Despite the fact that its prediction and eventual discovery was one of the brightest highlights in hadron physics, not much is known about the  $\Omega^-$  properties and the mechanism of  $\Omega^-$  production. Here are some basic facts:

- In 1962, Gell-Mann and Neèman predicted a new baryon,  $\Omega^-$ , with  $S = -3$ ,  $J^P = 3/2^+$ , and a mass of about 1670 MeV [2].
- The  $\Omega(1670)^-$  observation in 1964 at BNL triumphantly confirmed the hypothesis of  $SU(3)_F$ . The unambiguous discovery in both production and decay was reported in Ref. [3]. They scanned more than 100k bubble chamber pictures with 5–10  $K^-$  per picture and found a single and unique  $\Omega^-$ -event.
- The quantum numbers follow from the assignment of the particle to the baryon decuplet. Ref. [4] ruled out  $J = 1/2$  and found consistency with  $J = 3/2$ . The BaBar Collaboration measured the spin of the  $\Omega^-$  using  $\Xi_c^0 \rightarrow \Omega^- K^+$  and  $\Omega_c^0 \rightarrow \Omega^- K^+$ ,  $\Omega^- \rightarrow \Lambda K^-$  events. Under the assumption that the charm baryons have spin 1/2, as expected from the quark model, the angular distribution of the  $\Lambda$  from  $\Omega$  decay is consistent with spin assignment 3/2 for the  $\Omega^-$  and inconsistent with all half-integer spin assignments [5].
- Cross sections of  $\Omega(1670)^-$  production have been measured using kaon beams. The ANL experiment measured the  $K^- p \rightarrow \Omega^- X$  cross section at 6.5 GeV as  $\sigma_t =$

$1.4 \pm 0.6 \mu b$  [6]. The experiment SLAC E-135 measured the forward differential cross section for  $K^-p \rightarrow \Omega^- X$  at 11 GeV [7]. Experiment SLAC BC-073 sought  $\Omega^-$ -photoproduction in the  $\gamma p \rightarrow \Omega^- X$  reaction at 20 GeV, and provided only an upper limit of  $\sigma_t < 17$  nb [8].

Although there have been no experimental data on the photoproduction of  $\Omega^-$ , other than the upper limit set by the SLAC experiment [8], various theoretical models by Roberts, Afanasev, and Shklyar have provided predictions of cross sections of  $\Omega^-$  photoproduction, typically around 0.3 nb. These predictions will be discussed in detail in later sections. Therefore, we believe CLAS12 has a unique opportunity to produce long-awaited new data on  $\Omega^-$ -resonances.

Our physics goals for the studies of  $\Omega^-$  states are:

- to obtain a first measurement for the cross section for  $\gamma p \rightarrow \Omega^- K^+ K^+ K^0$ ,
- to study the reaction mechanism for  $\Omega^-$  in photoproduction (note that the  $\Omega^-$  is the first baryon with constituent quarks not inherited from the target proton);
- to search for other excited  $\Omega^-$  states (only the  $\Omega^-(2250)$  state is rated with at least three stars in the PDG, while neither the  $\Omega(2380)^-$  nor the  $\Omega(2470)^-$  have not been firmly established (Table 1)).

State	PDG rating	Width (MeV)	$J^P$
$\Omega^-$	****		$\frac{3}{2}^+$
$\Omega(2250)^-$	***	$55 \pm 18$	?
$\Omega(2380)^-$	**	$26 \pm 23$	?
$\Omega(2470)^-$	**	$72 \pm 33$	?

TABLE I: Well established Cascade resonances [1].

Various theoretical models by Roberts, Afanasev, and Shklyar have provided predictions of cross sections of  $\Omega^-$  photoproduction, typically around 0.3 nb. (These predictions will be discussed in detail in later sections.) Therefore, we believe CLAS12 has a unique opportunity to produce long-awaited new data on  $\Omega^-$ -resonances in photoproduction.

## B. Missing Cascade States

### 1. Current status of the cascade states

Constituent quark models predict the existence of a cascade state corresponding to each  $N^*$  and  $\Delta^*$  resonance. The relativised quark model with chromodynamics of Isgur and Capstick [9] predicts a total of 44 cascade states below 2.5 GeV. Current experimental verification of these predictions is badly lacking. Overall, only 6 cascade states are listed with three or four stars in [1], with only three of them have their quantum numbers  $J^P$  considered as determined (Table II).

State	PDG rating	Width (MeV)	$J^P$
$\Xi(1320)$	****		$\frac{1}{2}^+$
$\Xi(1530)$	****	9.5	$\frac{3}{2}^+$
$\Xi(1690)$	***	< 30	$\frac{1}{2}^-?$
$\Xi(1820)$	***	24	$\frac{3}{2}^-$
$\Xi(1950)$	***	60	?
$\Xi(2030)$	***	20	$\frac{5}{2}^?$

TABLE II: Well established cascade resonances [1].

In the past two decades, there have been no new cascade states discovered. The WA89 Collaboration [10] observed the  $\Xi(1690)$  in  $\Xi^0(1690) \rightarrow \Xi^- \pi^+$  decay while the  $\Xi(1690)$  has previously only been observed to decay largely to  $\Lambda/\Sigma K^-$  and  $\Lambda \bar{K}^0$  [11–13]. The W89 analysis of  $\Xi^0(1690) \rightarrow \Xi^- \pi^+$  decays suffered from combinatorial background from the inclusive reaction of  $\Sigma^-(C, Cu) \rightarrow \Xi^- \pi^+$  (Fig. 1), which lowered the significance of the result. In CLAS12, however, the exclusive reconstruction of reaction such as  $\gamma p \rightarrow K^+ K^+ K^- \Lambda$  or  $\gamma p \rightarrow K^+ K^+ \pi^- \Xi^0$  is expected to considerably reduce the combinatorial background underneath the reconstructed hyperon signals. This CLAS12 data sample would also be used to simultaneously measure the different decay modes of excited cascade resonances, thereby obtaining precise branching ratio values. Further experimental validation of the apparent suppression of the  $\Xi^* \rightarrow \Xi \pi$  decay, and detailed studies of excited cascade states that decouple from  $\Xi \pi$ , are essential to understand the properties of the cascade spectrum

and to shed light on the cause of their unusually narrow widths. In addition, this same data sample would be used to search for new excited  $\Xi$  states.

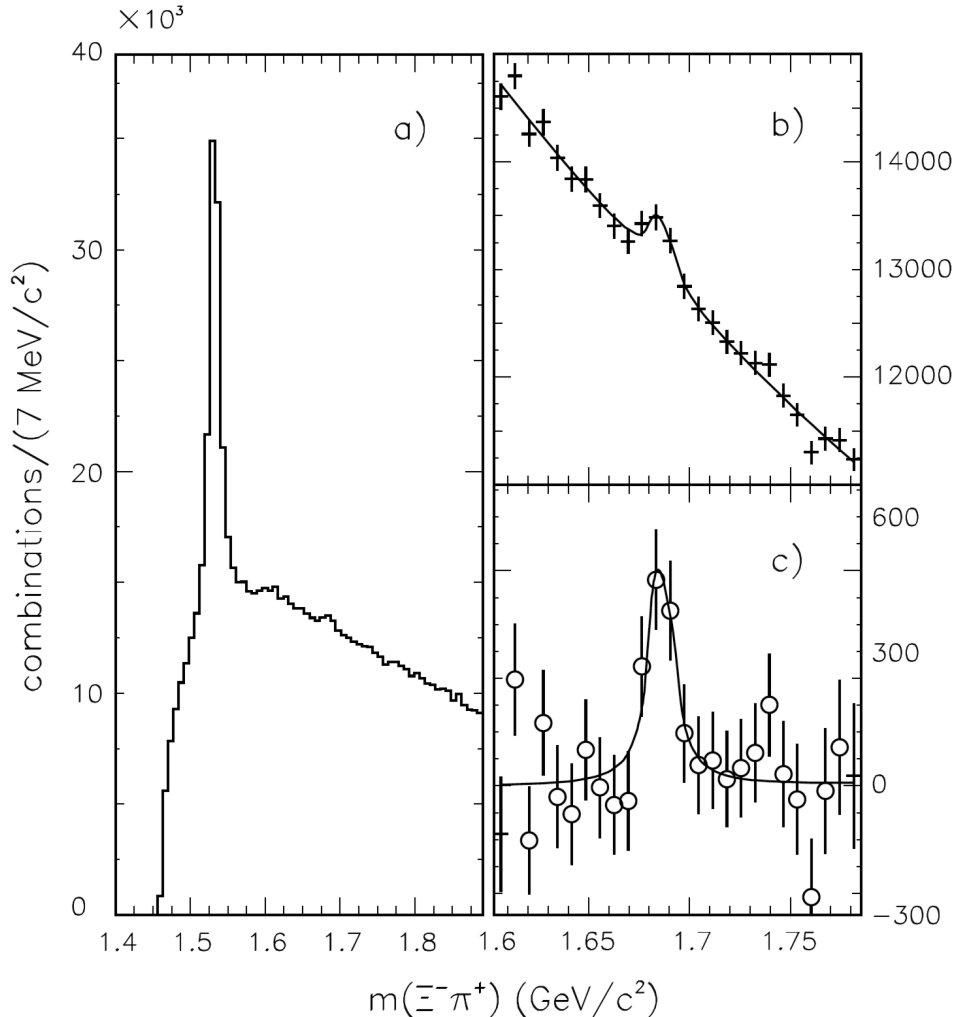


FIG. 1: Invariant mass distribution of the  $\Xi^- \pi^+$  combinations in the reaction of  $\Sigma^-(C, Cu) \rightarrow \Xi^- \pi^+$  [10]. a) The  $\Xi^0(1530)$  and  $\Xi^0(1680)$  mass region; b) The  $\Xi^0(1690)$  mass region only; c) the  $\Xi^0(1690)$  mass region after background subtraction.

The spectrum of cascade resonances is an integral part of the baryon physics. In the search for the missing nucleon resonances, a major difficulty is the overlapping of many broad states, which requires coupled-channel analysis as well as sophisticated partial wave analysis in order to extract their quantum numbers. In the case of cascade resonances, they are typically much narrower (Tabel II), and comparatively easier to identify. The main problem for the search for missing cascade states has always been producing them

State	$BR(\rightarrow \Lambda \bar{K})$	$BR(\rightarrow \Sigma \bar{K})$	$BR(\rightarrow \Xi \pi)$
$\Xi(1530)$			100%
$\Xi(1690)$	seen	seen	seen
$\Xi(1820)$	large	small	small
$\Xi(1950)$	seen	seen?	seen
$\Xi(2030)$	20%	80%	small

TABLE III: Branching ratio of excited Cascade resonances [1].

due to the small cross sections. Recent CLAS data established that the lowest excited cascades such as  $\Xi(1320)$  and  $\Xi(1530)$ , can be produced copiously for photon energies 1-2 GeV above threshold using a real photon beam at high luminosity. Depending on the production mechanisms [14, 15] the sharp drop in cross section exhibited by the  $S = -1$  hyperons (such as the  $\Lambda$ ) may not be present for the cascade whose cross section might tend to stay high for photon energies 1-2 GeV above threshold. This effect may counterbalance the typically one or two orders of magnitude lower cross section of cascade compared to that of the singly-strange hyperons.

The cross section of  $\Xi^-(1320)$  in the exclusive reaction of  $\gamma p \rightarrow K^+ K^+ \Xi^-(1320)$  was observed to increase from the nb level around  $E_\gamma = 3$  GeV to around 10 nb at 4 GeV [14]. Phenomenological models that hypothesize intermediate hyperons as the parent particle of the  $\Xi$ , also do not predict the drop-off of cross sections at higher energies [15]. Although recently published CLAS results (from the  $g11$  experiment consist of data using mostly photon energies below 4 GeV, a recent CLAS experiment (E05-017, also called  $g12$  in this document), has collected even higher statistics of cascade data, with beam energies up to 5.4 GeV (This CLAS experiment has an estimated luminosity of  $28 \text{ pb}^{-1}$  for  $E_\gamma > 4.4$  GeV, using a 40 cm long liquid hydrogen target.)

Among the states listed in Table 3, there is recent evidence to suggest that the  $\Xi(1690)$  is a  $J^P = \frac{1}{2}^-$  particle, from the decay  $\Lambda_C^+ \rightarrow \Xi^- \pi^+ K^+$  [16]. However, extracting this result required assumptions about the  $J^P$  of  $\Lambda_C^+$  as well, making a further independent measurements very desirable. This is a state that is of particular interest, as CLAS12 is well suited to investigate its production via different decay channels.

For example, the  $\Xi^0 \pi^-$  decay of  $\Xi^0(1690)$  can be investigated via the reaction  $\gamma p \rightarrow$

$K^+K^+\pi^-(\Xi^0)$ . In fact, this reaction has been analyzed recently using the  $g12$  data set. The three charged particles in the final state are identified by CLAS, while the  $\Xi^0$  is reconstructed using the missing-mass technique (Fig. 2). The  $\Xi^0$  signal is clearly visible above a smooth background, mostly from events with pions misidentified as kaons. However, these existing data are not ideal for the investigation of excited cascade states such as the  $\Xi^-(1690)$ , as most of the  $\Xi^0\pi^-$  events are expected to arise from the  $\Xi^-(1530)$  decay. The expected low cross section of  $\Xi^-(1690)$  for  $E_\gamma < 6$  GeV would make it difficult to observe it in the existing data. In CLAS12, not only can the  $\Xi^-(1690)$  be detected from its  $\Xi^0\pi^-$  decay, but also its  $Y\bar{K}$  decay. As discussed later, the assignment of  $J^P = \frac{1}{2}^-$  to the  $\Xi^-(1690)$  [16] can also be confirmed using the double moments analysis by reconstructing the whole decay chain.

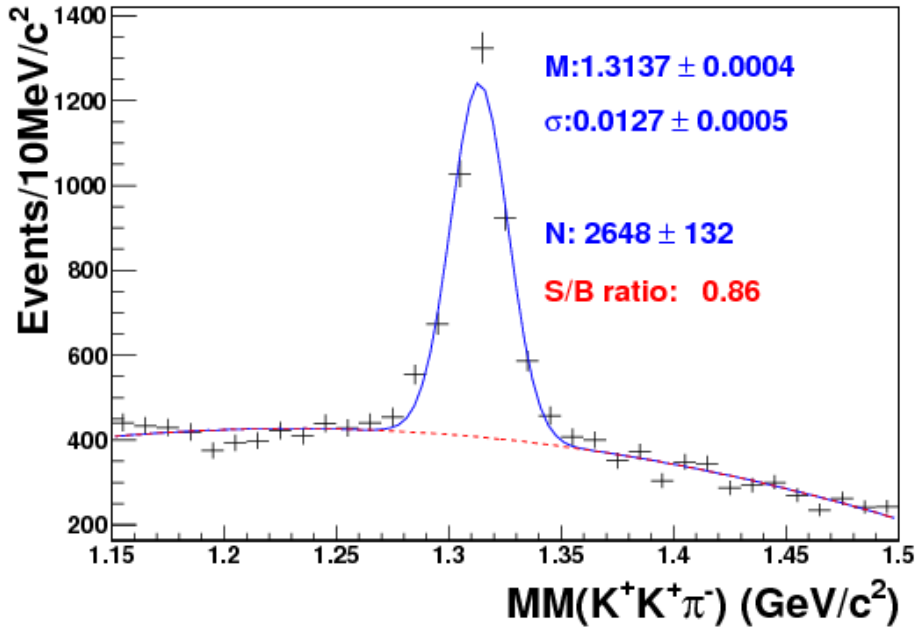


FIG. 2: The missing mass spectrum of the  $\gamma p \rightarrow K^+K^+\pi^-(X)$ , from the  $g12$  experiment. The included photon energy range here is 3.3 GeV to 5.4 GeV. Various offline corrections, such as momentum corrections and beam energy corrections have not been finalized for this experiment, and the parameters of the signal are expected to improve significantly.

## 2. Mass splitting of $\Xi$ doublets

Another unique feature of cascade physics is the possibility to perform the measurement of the mass splitting for multiple cascade doublets. In order to access the fundamental parameters of QCD such as quark masses, it is essential to accurately determine the mass splitting of multiple baryon isospin multiplets. The average of the baryon ground state isospin multiplet ( $N, \Sigma, \Delta, \Xi, \Sigma_c$ , and  $\Xi_c$ ) mass differences yields a value of  $m_u - m_d = +2.8 \pm 0.3$  MeV [17]. However, the  $\Xi$  ground state doublet mass splitting is the most intriguing one. The global average of the mass difference between the  $\Xi^0$  and  $\Xi^-$  doublet is  $6.48 \pm 0.24$  MeV according to the PDG [1], significantly higher than that of the other baryon ground state multiplets. Recent QCD lattice calculations yield a result of  $5.68 \pm 0.24$  MeV [18], while a calculations based on radiative correction to the quark model gives a result of 6.10 MeV [19]. Experimentally, however, it is important to point out that only one measurement of the  $\Xi^0$  mass, by the NA48 Collaboration, has more than 50 events [20]. It seems plausible that this lone high statistics measurement of the  $\Xi^0$  mass could be too low. In fact, recent CLAS measurements of the mass splitting of the ground state ( $\Xi^-, \Xi^0$ ) doublet is  $5.4 \pm 1.8$  MeV [14], which is lower than the global average. Nevertheless, the CLAS results did suffer from a lower statistical sample of  $\Xi^0$  events, and could not make a definite statement on the  $\Xi$  ground state doublet mass splitting.

In addition to producing the neutral cascade from reactions such as  $\gamma p \rightarrow K^+ K^+ \pi^- \Xi^0$ , it is also possible to access these states via the reaction  $\gamma p \rightarrow K^+ K^0 \Xi^0$ , with the  $K^0$  reconstructed from the  $\pi^+ \pi^-$  decay of the  $K_s$  component. In the reaction  $\gamma p \rightarrow K^+ K^0(X)$ , the strangeness of the detected  $K^0$  is not defined, and therefore the background from pions misidentified as kaons could be significant. However, due to the narrowness of the cascade resonances, it still should be feasible to observe them from the  $K^+ K^0$  missing mass spectrum. In fact, existing data from g11 ( $E_\gamma$  up to 3.8 GeV) have already demonstrated this possibility, where the  $\Xi^0$  is clearly visible in the  $K^+ K^0$  missing mass spectrum (Fig. 3).

CLAS12 would be well suited to perform multiple mass splitting measurements for a series of  $\Xi^*$  doublets, further enhancing our knowledge of the  $u, d$  quark mass difference. This is largely due to the narrowness of the  $\Xi^*$  resonances, the improved acceptance and luminosity of CLAS12 over CLAS, and of course, the higher beam energy. This kind of multiple measurements of mass splitting of different baryon multiplets would not have been

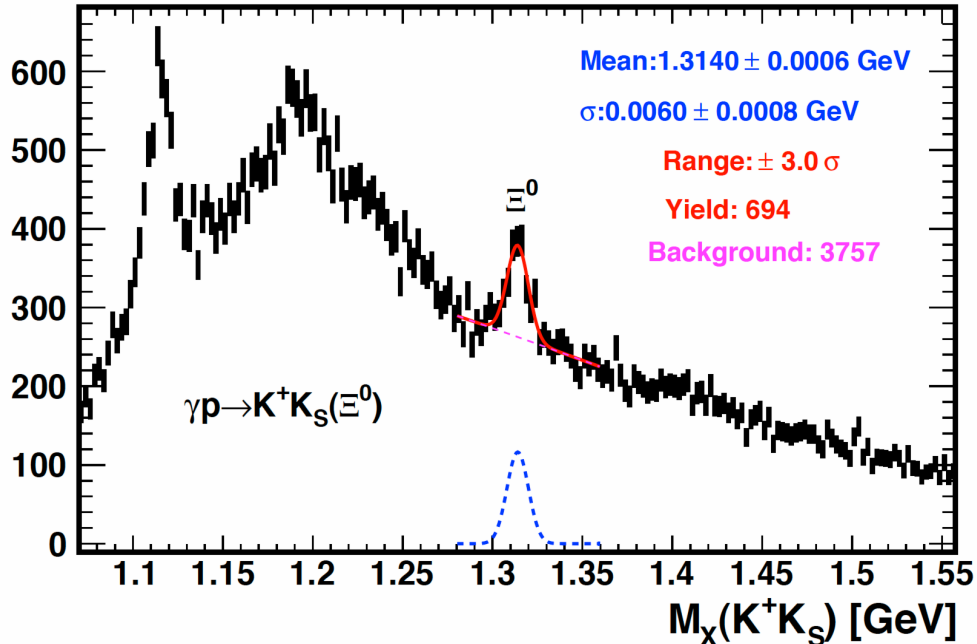


FIG. 3: The missing mass spectrum of the  $K^+K_s$  system for a proton target, from the  $g11$  experiment. The  $K_s$  is identified from the  $\pi^-\pi^+$  invariant mass.

possible in other sectors such as the  $N^*$  and  $Y^*$  resonances, due to their typically larger widths and the associated uncertainties.

### C. Cascade Polarization

Hyperon polarization has generated much interest in the hadron physics community. Recently CLAS has produced several interesting results on the polarization of  $S = -1$  hyperons. In photoproduction data, Bradford *et al.* have shown that the  $\Lambda$  is 100% polarized with a circularly polarized photon beam [21] (Fig. 4, while the induced polarization of  $\Lambda$  in the reaction of  $\gamma p \rightarrow K^+\Lambda$  is shown to change signs as a function of the  $K^+$  center-of-mass angles [22] (Fig. 5)). Similarly, due to the self-analyzing nature of the  $\Xi(1320)$  weak decay, the polarization can be measured in various photo-nucleon reactions, with or without target/beam polarization. Such observables are important for the understanding of the production mechanism of cascade resonances in general. Furthermore, compared with the case of the  $\Lambda(uds)$ , whose polarization is likely from the strange quark, with a small contribution from the  $(ud)$  diquark, the polarization mechanism of the  $\Xi((u/d)ss)$ , however,

might be totally different. The cascade polarization more likely comes from the valence quark ( $u/d$ ) instead of the ( $ss$ ) diquark. If this is true, then the recoil polarization of the  $\Xi$  should be negligible in photoproduction data without beam/target polarization, opposed to the sizable recoil polarization observed for  $\Lambda$ . It is also possible to use the polarization of the  $\Xi(1320)$  in photoproduction on a polarized nucleon target to study the different contributions of valence quarks to the nucleon polarization, which would be complementary to the results using electron scattering.

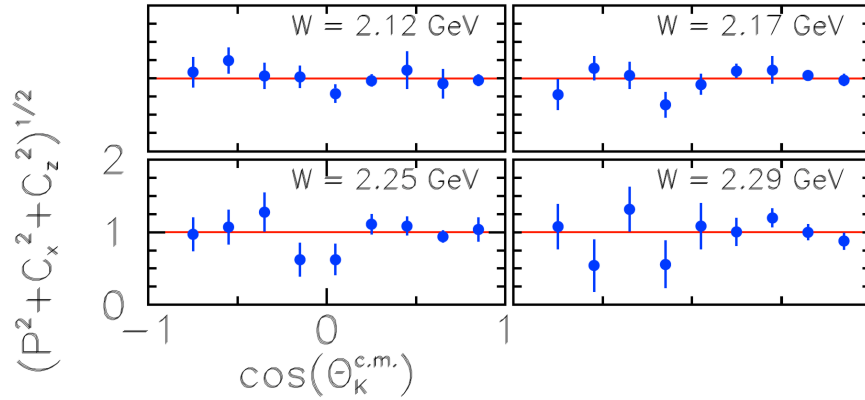


FIG. 4: The magnitude of the  $\Lambda$  hyperon polarization  $R_\Lambda = \sqrt{P^2 + C_x^2 + C_z^2}$  is shown to be consistent with unity [21].

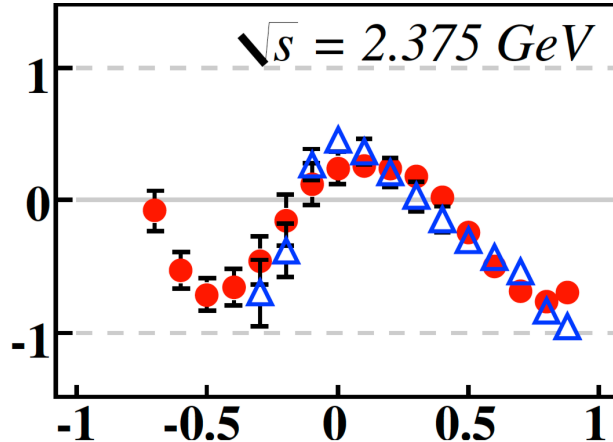


FIG. 5: The induced  $\Lambda$  polarization  $P_\Lambda$  is shown to change signs as a function of  $\cos\theta^{c.m.}$  [22].

Because of parity conservation in the production of  $\Xi^-$  in the reaction  $\gamma p \rightarrow K^+ K^+ \Xi^-(1320)$ , if there is no beam or target polarization, the only direction the  $\Xi^-$  can be

polarized is normal to the production plane, defined by the target, beam, and the outgoing  $\Xi^-$  (Fig. 6). For a weakly decaying particle such as the  $\Xi^-(1320)$ , the polarization can be measured via its decaying angular distribution, which takes the form of

$$I(\theta) = A(1 - \alpha P \cos(\theta)). \quad (1)$$

For the  $\Xi^-(1320)$ , the value of  $\alpha$  is -0.456, and  $P$  denotes the polarization. The polarization  $P$  can be also determined by

$$P = -\frac{2 N^+ - N^-}{\alpha N^+ + N^-}, \quad (2)$$

with  $N^+$  denoting events in the forward direction, and  $N^-$  in the backward direction.

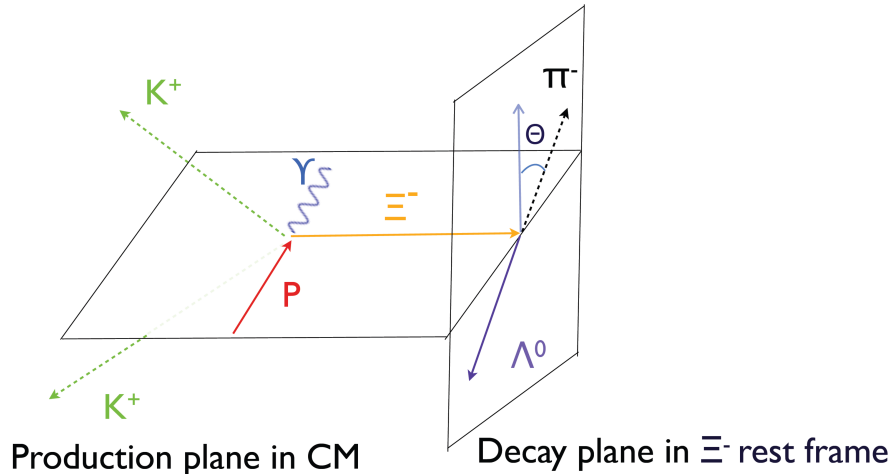


FIG. 6: Illustration of the  $\Xi^- \rightarrow \Lambda\pi^-$  decay for the polarization measurement in the reaction  $\gamma p \rightarrow K^+ K^+ \Xi^-(1320)$ . The production plane is defined by the beam, target, and the outgoing  $\Xi^-$ . The  $\pi^-$  angle is measured in the  $\Xi^-$  rest frame, with the  $z$ -axis for the polarization measurement defined by the normal to the production plane.

If there is beam or target polarization, then presumably some of the initial polarization can be transferred to the  $\Xi^-(1320)$ , and a measurement of the in-plane polarization of the  $\Xi^-(1320)$  can become a very useful tool to probe the production mechanism of  $\Xi$  baryons. For example, recent photoproduction data of  $\Lambda$  in the reaction of  $\gamma p \rightarrow K^+ \Lambda$  has shown that the polarization of a circularly polarized photon beam is almost exclusively transferred to the hyperon [21]. If the production mechanism for  $\Xi$  is similar to that of the  $\Lambda$ , then it is not inconceivable that some of the beam polarization is transferred to the  $\Xi$ . On the other hand,

in a conventional di-quark picture of baryon resonances, the polarization mechanisms of the  $\Lambda$  and  $\Xi$  could be fundamentally different as discussed earlier. If it is true that most of the  $\Xi$  polarization is from the valence quark contribution, then the difference in  $\Xi$  polarization between an unpolarized and polarized photon beam should be very small, provided that there is no target polarization.

The proposed program will measure the induced  $\Xi^-$  polarization and the beam polarization transfer, since the quasi-real photon polarization could be determined on an event-by-event basis. The comparison between  $\Lambda$  and  $\Xi^-$  polarizations can be made, and the production mechanism can be further explored. As demonstrated by the existing CLAS data from the  $g11$  experiment (Fig. 7), extremely clean signals for  $\Xi^- \rightarrow \Lambda\pi^-$  can be identified, due to the fact that there are two narrow resonances providing kinematic constraints. In fact, such an unique feature is one of the main reasons to focus on this channel, as it simplifies the analysis of the decay angular distributions greatly and makes the extraction of polarization variables much less susceptible to background contamination. As a first exploratory look, the decay angular distributions of these extremely clean samples of  $\Xi^- \rightarrow \Lambda\pi^-$  events are analyzed, and the preliminary  $\Xi^-(1320)$  polarization measurements, as a function of photon energy, are shown in Fig. 8. These preliminary results are consistent with zero polarization, which is close to our expectation due to no beam polarization. They are already notably different from the  $\Lambda$  induced polarization measured recently by CLAS [22]. However, it is also possible that our preliminary results are due to integrating over kinematic variables, such as the  $\Xi^-$  angle in the center-of-mass (CM) frame.

The photon beam was not polarized during the  $g11$  experiment. On the other hand, the  $g12$  experiment was conducted with circular polarization up to 70% at the high energy end. It is possible that part of the polarization of the beam can be transferred to the  $\Xi^-$ , as is the case for  $\Lambda$  photoproduction ([21]) with a circularly polarized beam. If our conjecture that the  $\Xi^-$  polarization is mainly from the valence  $d$  quark, then the picture could be totally different. At the present time, the detailed analysis of the  $\Xi^-$  polarization in the  $g12$  experiment is still on-going, but the statistics is limited to study the relations between the cascade and beam polarizations as a function of different observables.

The proposed experiment will have one important advantage over these CLAS experiments: the polarization of the quasi-real photon can be determined on an event-by-event basis at CLAS12 with the addition of the forward tagger (see the discussion in the later

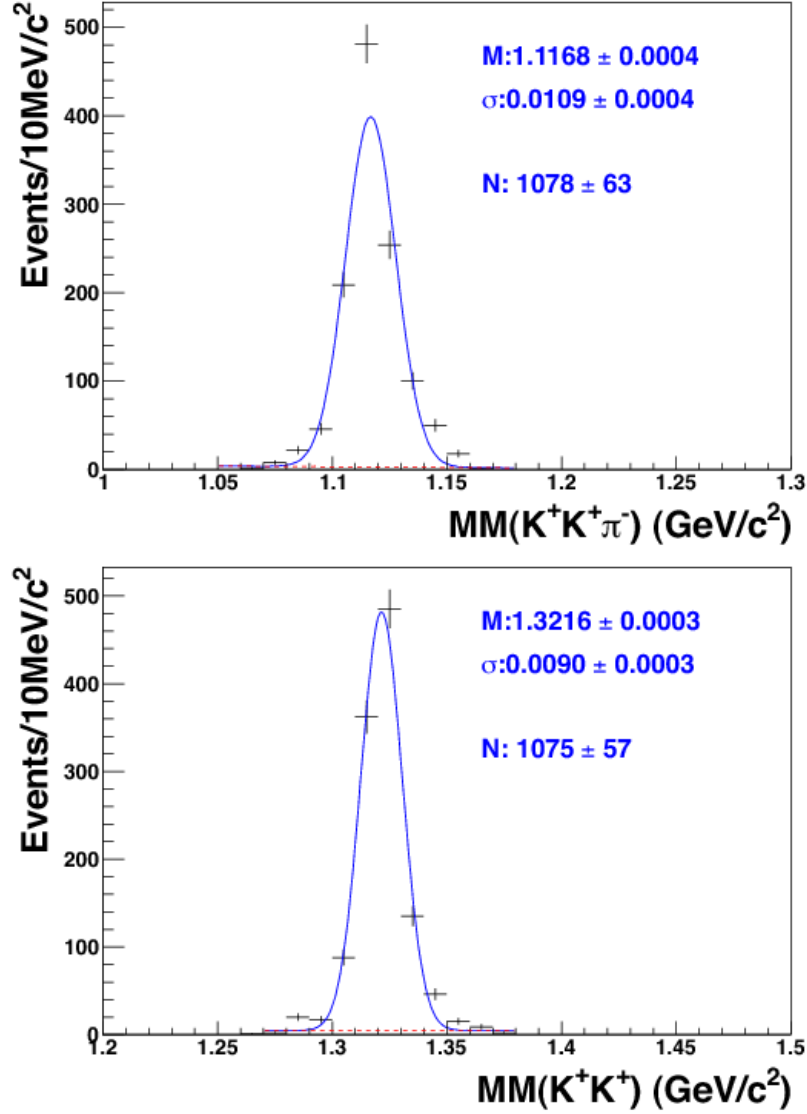


FIG. 7: Top: The missing mass spectra of the  $K^+K^+\pi^-$  system for a proton target. Events corresponding to the  $\Xi^-$  signal are selected; Bottom: The missing mass spectra of the  $K^+K^+$  system for a proton target. Events corresponding to the  $\Lambda$  signal are selected. The data were collected by the  $g11$  experiment, and the photon beam is unpolarized. The included photon energy range here is between 3.0 GeV and 3.8 GeV.

sections), enabling a detailed study of the relation of the  $\Xi^-$  and beam polarizations in photoproduction for the first time.

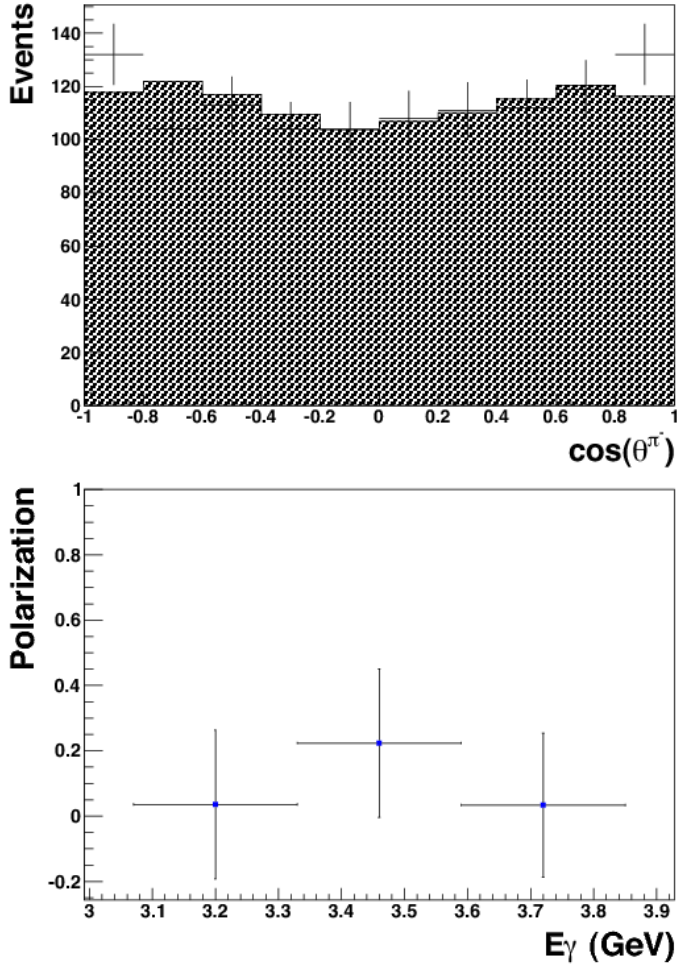


FIG. 8: Top: The integrated decay angular distribution of the  $\Xi^-$  decay. The angle between the  $\pi^-$  momentum and the normal to the production plane is  $\theta^\pi$ . The shaded histogram is based on a simulation of the differential cross sections results reported in Ref. [14]. The included photon energy range here is between 3.0 GeV and 3.8 GeV; Bottom: Preliminary results of the calculated  $\Xi$  polarization perpendicular to the production plane is consistent with zero within the uncertainties. Errors are statistical only. An estimated systematic uncertainty of 10% is not shown. The data were collected by the  $g11$  experiment with an unpolarized photon beam.

#### D. $\Omega N$ and $\Xi N$ Elastic Scattering

The fact that all ground-state hyperons decay weakly allows one to consider the possibility that they can interact with a second proton in the target. This secondary interaction takes place via the strong interaction, and therefore may occur often enough to observe with the CLAS detector.  $SU(3)_F$  symmetry dictates that the cross section for hyperon-nucleon

scattering should be comparable to that of  $NN$  scattering; a simple model [23] gives the relation

$$\sigma(\Xi^-p) + \sigma(pp) = 2\sigma(\Lambda p),$$

which makes it possible to estimate the event rates we can expect in an experiment with CLAS12.

A detailed study of the interaction of the  $\Xi$  hyperons with the nucleon may help to illuminate  $SU(3)_F$  symmetry breaking in the baryon-baryon interaction. A particular process,  $\Xi^-p \rightarrow \Lambda\Lambda$ , may point to the existence of the  $H$  dibaryon, which has not yet been observed [24, 25], or allow the first direct measurement of the parity of the ground-state  $\Xi^-$  [26].

The existing data on hyperon-nucleon scattering is sparse for  $S > 1$ , consisting primarily of a few events seen in high-energy bubble-chamber experiments done in the 1970s [27–30]. Recently, a new measurement at lower energies was attempted using a scintillating fiber target [31]. Out of more than six thousand  $\Xi^-$  events seen in the  $p(K^-, K^+)\Xi^-$  process, a single candidate event for the elastic scattering process  $\Xi^-p \rightarrow \Xi^-p$  remained, leading to an upper limit of 24 mb. Quality data on  $\Xi^-p$  scattering would help to constrain theoretical models for this process and help to illuminate the nature of the hyperon-nucleon interaction [32–36].

### III. THEORETICAL MODELS FOR $\Omega^-$ PHOTOPRODUCTION CROSS SECTIONS

In this section, the estimation of photoproduction cross sections for  $\Omega^-$ -photoproduction on a nucleon will be discussed, using a variety of models.

#### A. Vector-Meson Dominance Model

Afanasev considers  $\Omega^-$ -production on a proton target. The photoproduction amplitude in the Vector-Meson Dominance (VMD) approximation may be written

$$f(\gamma p \rightarrow \Omega^- X)|_{VMD} = (e/f_\rho)f(\rho^0 p \rightarrow \Omega^- X) + (e/f_\omega)f(\omega p \rightarrow \Omega^- X) + (e/f_\phi)f(\phi p \rightarrow \Omega^- X), \quad (3)$$

where the photon-vector meson couplings  $f_{\rho\omega\phi}$  can be obtained from the measured partial decay widths of vector mesons  $\Gamma(\rho, \omega, \phi \rightarrow e^+e^-)$  [1]. In the following, we make an assumption that the leading contribution to  $\Omega$ -production is due to the intrinsic strangeness component of the photon. In the constituent quark model, the  $\phi$ -meson is primarily an  $s\bar{s}$ -pair, providing strange quarks in the incident photon beam. Therefore,

$$f(\gamma p \rightarrow \Omega^- X)|_{\phi MD} \sim (e/f_\phi)f(\phi p \rightarrow \Omega^- X). \quad (4)$$

Then, the photoproduction cross section is

$$f(\gamma p \rightarrow \Omega^- X)|_{\phi MD} \sim (\alpha/\alpha_\phi)\sigma(\phi p \rightarrow \Omega^- X). \quad (5)$$

Here,  $\alpha$  is a fine structure constant, while the value  $\alpha_\phi = f_\phi^2/4\pi = 14.3 \pm 0.5$  is obtained from the partial width  $\Gamma(\phi \rightarrow e^+e^-) = (1.27 \pm 0.04)$  keV [1]. Using an additive quark model, we further relate cross sections of  $\phi p \rightarrow \Omega^- X$ ,  $K^- p \rightarrow \Omega^- X$ , and  $K^+ p \rightarrow \Omega^- X$  processes by

$$f(\phi p \rightarrow \Omega^- X) = [\sigma(K^- p \rightarrow \Omega^- X) + \sigma(K^+ p \rightarrow \Omega^- X)]/2. \quad (6)$$

Experimental data exist only for the  $K^- p \rightarrow \Omega^- X$  process [7]. Using these data, we are able to estimate the photoproduction cross sections at the matching momenta, assuming the production mechanism shown in Fig. 9. We consider the numbers obtained in this model to be upper limits. Based on this model, we estimate that, for the 11-GeV photon beam, we can anticipate the  $\Omega^-$ -baryon inclusive photoproduction cross section at the level of  $\sigma_t = 0.5 - 1$  nb. This inclusive cross section can be translated into an exclusive prediction. We estimate the exclusive cross section for  $\gamma p \rightarrow \Omega K K K$  at  $\sigma_t = 0.4 - 0.5$  nb. This follows from two independent arguments:

- Using Ref. [7] for the  $K^- p \rightarrow \Xi^- X$  cross section and  $\phi^-$  VMD, we get  $\sigma_t \sim 40$  nb for inclusive  $\gamma p \rightarrow \Xi^- X$ . The CLAS Collaboration obtained  $\sigma_t \sim 15$  nb for exclusive  $\gamma p \rightarrow \Xi^- K K$  at photon energies near  $E_\gamma = 5$  GeV - energies far enough from the production threshold [14]. It leads to reduce our previous VMD-based estimate (1 nb) by a factor of 2.5 for  $\Xi^-$ . Assuming the same reduction factor for  $\Omega^-$ , the exclusive cross section of  $\gamma p \rightarrow \Omega^- K K K$  is therefore estimated to be  $\sigma_t \sim 0.4$  nb.
- Inclusive cross sections for  $K^- p \rightarrow \Xi^- X$  and  $K^- p \rightarrow \Omega^- X$  at 11 GeV appear to be in the approximate ratio 30:1 [7]. Let us assume the cross sections for  $\gamma p \rightarrow \Xi^- K K$

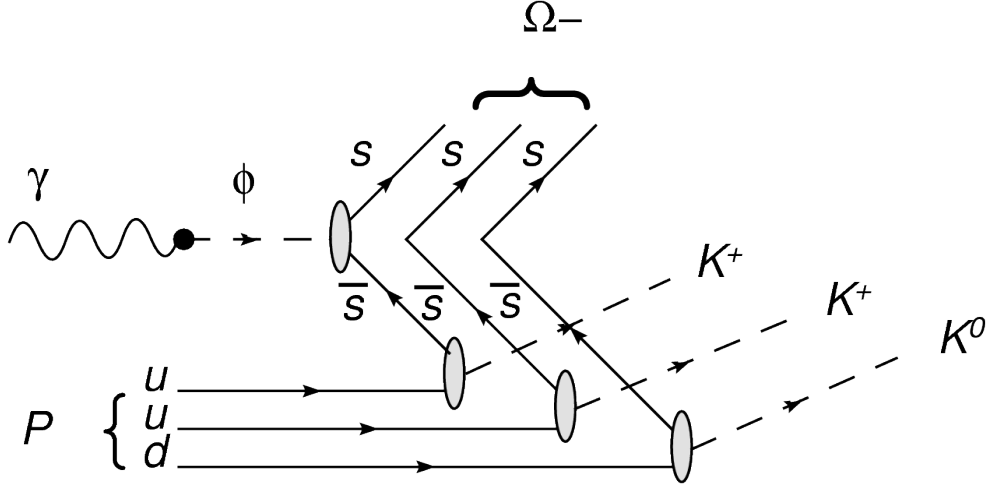


FIG. 9: Quark diagrams for the  $\Omega^-$  photoproduction in the VMD approach of Afanasev.

and  $\gamma p \rightarrow \Omega^- K K K$  are in the same ratio. The former is measured at CLAS to be  $\sigma_t \sim 15$  nb [14], then the exclusive  $\Omega^-$  cross section is a factor of 30 less, which is  $\sigma_t \sim 0.5$  nb. Note that VMD was not used here explicitly.

### B. Effective Lagrangian Model-1

The second prediction for the cross section for  $\gamma N \rightarrow K^+ K^+ K^0 \Omega^-$  is obtained by Roberts in a simple model based on a phenomenological Lagrangian. The model uses the diagrams shown in Fig. 10, where all permutations of external legs are included. This means that there are 24 diagrams like the first one, and another 18 like the second. The ground state nucleon,  $\Lambda$ ,  $\Sigma$  and  $\Xi$  and two excited  $\Xi$  with  $J^P = 1/2^+$  (masses of 1.91 and 2.14 GeV, respectively, taken from a quark model calculation [37]) are included in the calculation. The mesons are assumed to couple to the spin-1/2 baryons through a pseudoscalar coupling. Some of the required coupling constants are taken from a preliminary fit to CLAS data on photoproduction of the  $\Xi$  baryon. The couplings of the excited  $\Xi$ s to the ground state hyperons are obtained by assuming total widths of 50 MeV and branching fractions of 30% into each of the  $\Lambda K$  and  $\Sigma K$  channels. The results from this estimate are shown in Fig. 15. The dash-dotted curve is obtained with pair of signs for the couplings of the two  $\Xi$  resonances included in the calculation. The short dashed curve is obtained when the sign of one of those couplings is flipped with the magnitude unchanged. One can expect that inclusion of other

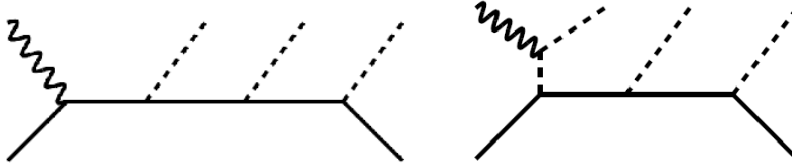


FIG. 10: Diagrams used in the calculation of the cross section for  $\gamma N \rightarrow KKK\Omega$ , in the phenomenological Lagrangian approach of Roberts.

contributions may further enhance the total cross-section for production of the  $\Omega^-$ , but total cross sections are expected to be at most a few nanobarns.

### C. Effective Lagrangian Model-2

A third approach by Shklyar is given for the calculation of the  $\Omega^-$ -photoproduction cross section (Fig. 11, which is similar to Fig. 10). The resonance production of  $S = -3$  baryons can be represented by a sequence of transitions  $\gamma p \rightarrow \Lambda^* \rightarrow \Xi^* \rightarrow \Omega^-$ , where kaons are emitted at each step. There are three additional diagrams obtained by permutations of the final kaon momenta in the diagram depicted in Fig. 11:  $(q_1 \leftrightarrow q_3)$ ,  $(q_2 \leftrightarrow q_3)$ , and  $(q_2 \rightarrow q_3, q_3 \rightarrow q_1, \text{ and } q_1 \rightarrow q_2)$ .

Here, we assume that the reaction goes through the excitation of the two heavy resonances  $\Lambda^*(3000)$  and  $\Xi^*(2370)$ . The PDG listings [1] indicate several heavy  $\Lambda^*$ - and  $\Sigma^*$ -states with masses close to 3 GeV. Most of their properties are unknown. Therefore, we will treat the  $\Lambda^*(3000)$  resonance with  $J^P = 1/2^+$  as a “generic” one assuming that it corresponds to overall possible contributions from both  $\Lambda^*$ - and  $\Sigma^*$ -hyperons. The model parameters are chosen as follows:  $m_{\Lambda^*(3000)} = 3$  GeV,  $\Gamma_t(\Lambda^*(3000)) = 200$  MeV,  $\text{Br}(\Lambda^*(3000) \rightarrow K^*(892)N) = 20\%$ , and  $\text{Br}(\Lambda^*(3000) \rightarrow K\Xi^*(2370)) = 10\%$ . The  $\Xi^*(2370)$  state is rated by two stars in the PDG listings and has a 10 % branching decay ratio to  $K\Omega^-$  and a 20% decay fraction to the “generic”  $K^*(892)\Lambda$  and  $K^*(892)\Sigma$  final states. The spin and parity of the  $\Xi^*(2370)$  are also unknown and calculations are also done assuming  $J^P = 1/2^+$ . The total width of  $\Gamma_t(\Xi^*(2370)) = 80$  MeV which is taken from the PDG [1]. The interaction Lagrangian is chosen as

$$L = g_{\Omega\Xi^*K} \left[ \bar{\Omega}(x) i\gamma_5 \Xi^{(*)}(x) \right] K(x) \quad (7)$$

$$\begin{aligned}
& + g_{\Lambda^* \Xi^* K} \left[ \bar{\Xi}^{(*)}(x) i \gamma_5 \Lambda^{(*)}(x) \right] K(x) \\
& + g_{\Lambda^* K^* N} \left[ \bar{N}(x) \sigma_{\mu\nu} \Lambda^{(*)}(x) \right] K^{(*)\mu\nu}(x) \\
& + \frac{e g_{K^* K \gamma}}{4m_K} \epsilon_{\mu\nu\rho\sigma} K^{(*)\mu\nu}(x) F^{\rho\sigma}(x) K(x) \\
& + \text{h.c.},
\end{aligned}$$

where the isospin indices are omitted. The coupling constants are calculated from the corresponding decay branching ratios. The  $K \Xi^* \Lambda^*$  and  $K \Xi^* \Omega$  vertices are dressed by the form factor

$$F_s(q^2) = \frac{\Lambda_s^4}{\Lambda_s^4 + (q_s - m_R^2)^2}, \quad (8)$$

where  $q_s$  is a momentum of the propagating baryon in the  $s$ -channel and  $m_R$  is the mass of the resonance. The form factor used at the  $t$ -channel vertex has the form

$$F_t(q^2) = \frac{\Lambda_t^4 + m_{K^*}^4}{\Lambda_t^4 + (t + m_{K^*}^2)^2}, \quad (9)$$

where  $t = (q_1 - k)^2$  for the diagram depicted in Fig. 11. The cutoff parameter is chosen to be  $\Lambda_s = \Lambda_t = 1.5$  GeV.

For the case of a resonance production mechanism, the exclusive  $\gamma p \rightarrow K^+ K^0 K^+ \Omega^-$  cross section is estimated to be about 0.5 nb at  $E_\gamma = 11$  GeV. This is a conservative estimate and inclusion of additional channels would lead to a larger total cross section. Measurements of invariant mass distributions can provide important information on the  $\Omega^-$  production process. The invariant mass distribution  $d\sigma dM_{q_3, p_\Omega}^2$  calculated in the case at hand is shown in Fig. 12. Here the notation  $M_{q_3, p_\Omega}^2 = (q_3 + p_\Omega)^2$  is adopted, where  $q_3$  is a kaon momentum. Due to symmetrization the charged kaons can be emitted at any vertex which corresponds to the different kinematical situations. The interplay between contributions where the charged kaons are emitted at the  $\Lambda^* \Xi^* K$  and  $\Xi^* \Omega^- K$  vertices leads to the broad structure in the  $M_{q_3, p_\Omega} = 2.2 - 2.6$  GeV invariant mass region with the dip around the  $\Xi^*(2370)$  resonance mass. The second peak at 2.9 GeV is due to the  $\Lambda^*(3000)$  excitation. Hence, the invariant mass distribution could shed light on the details of the  $\Omega^-$  production mechanism and distinguish between resonance and non-resonance contributions.

Additional information can be also obtained from the analysis of Dalitz-plots. To minimize the influence of 4-body phase space, a special choice of variables should be adopted, which however complicates the analysis. For the case of a strong resonance contribution,

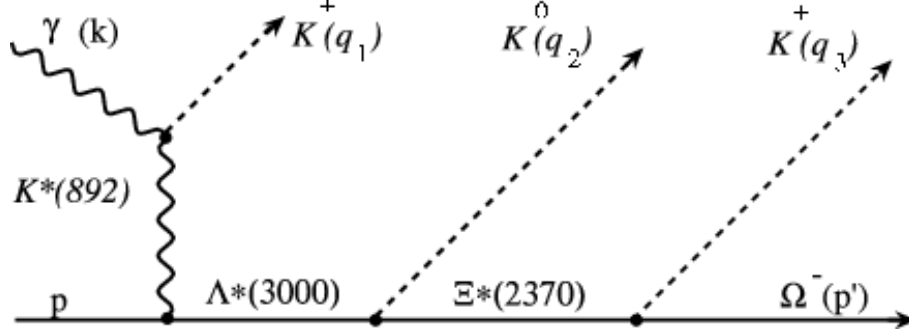


FIG. 11: Feynman diagram for the  $\gamma p \rightarrow K^+ K^0 K^+ \Omega^-$  transition in the effective Lagrangian approach of Shklyar.

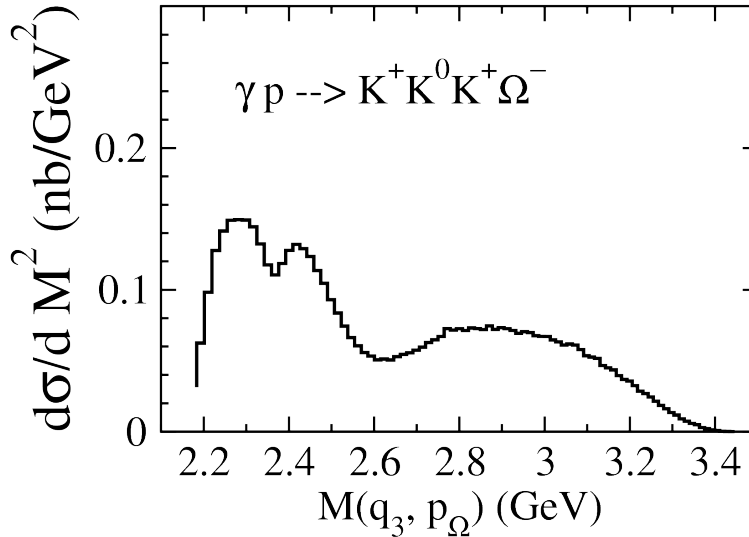


FIG. 12: Invariant mass distribution for the resonance production mechanism shown in Fig. 11.

one can use conventional Mandelstam variables. In Fig. 13 (right) the event distribution is shown as a function of  $(q_2 + p_b)^2$  and  $(q_3 + p_b)^2$ , where  $q_2$  is the  $K^0$ -momentum; the effect of the phase space is demonstrated in Fig. 13 (left). One can clearly see a resonance contribution coming from the  $\Xi^*$  excitation. The analysis of events can also give information on symmetry properties of the production amplitude. The result in Fig. 13 is obtained assuming a neutral  $\Lambda^*(3000)$  resonance contribution. In the case of isospin- $\frac{3}{2}$  intermediate states, one can expect the situation where the  $K_0$  is also emitted at the  $t$ -channel vertex, which might lead to a fully symmetric production amplitude. The corresponding event distribution is presented in Fig. 14.

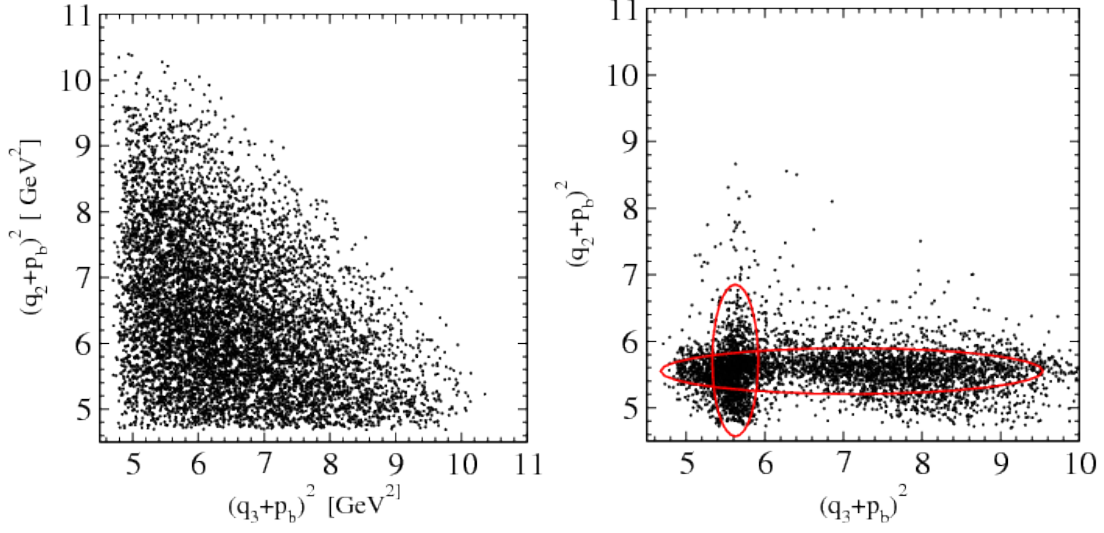


FIG. 13: Dalitz plot: phase space only (left),  $\gamma p \rightarrow K^+ K^0 K^+ \Omega^-$  reaction (right); the regions with the strong  $\Xi^*$  state contributions are shown by the red ellipses.

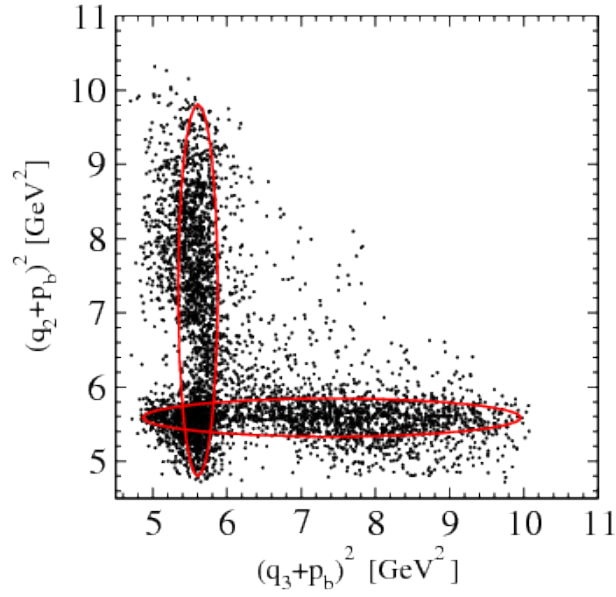


FIG. 14: Dalitz plot for the fully symmetric  $\gamma p \rightarrow K^+ K^0 K^+ \Omega^-$  reaction.

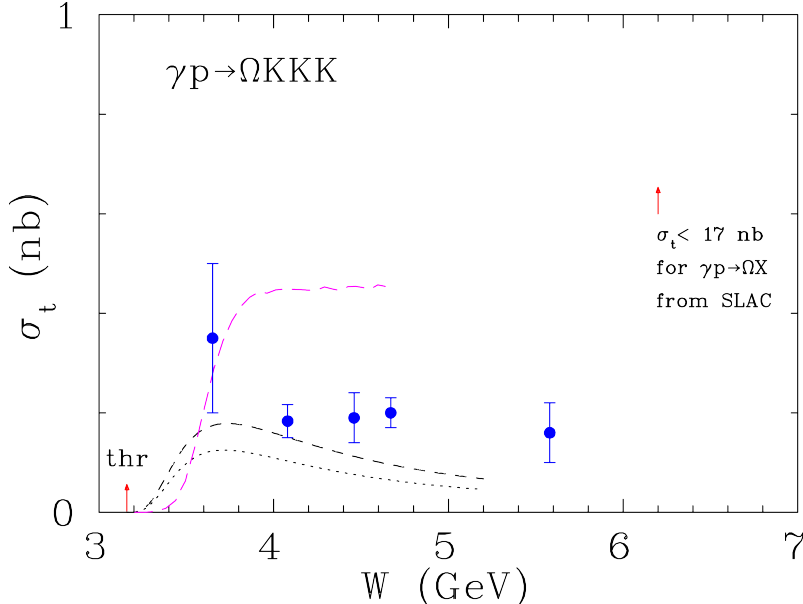


FIG. 15: Total exclusive cross section for  $\Omega^-$  photoproduction. The blue filled circles show the conservative phenomenological translation of the hadronic cross sections into those for photoproduction. The dash-dotted (short dashed) curve shows phenomenological Lagrangian-1 calculations (see text for details). The dotted curve presents  $\Omega^-$  production using a different Lagrangian-2 approach. The red arrow indicates the threshold  $W = 3.16$  GeV ( $E_\gamma = 4.85$  GeV).

#### IV. CROSS SECTION ESTIMATES

##### A. Cross Section Estimates for $\Omega^-$

Overall, Fig. 15 shows the cross section estimate as obtained for the  $\Omega^-$  photoproduction on the proton. Near threshold, the cross section is small, as expected, but quickly grows into the nanobarn range (or tens of nanobarns, depending on the coupling constants). A cross section of a few nanobarns in the energy range of interest seems to be a safe estimate. The critical feature is that all four estimations are consistent with each other. Clearly, the effective Lagrangian approach may not be applicable very far from threshold, as the cross sections continue to rise but we have no idea how strongly energy-dependent to make them.

One can estimate [38] that the photoproduction rate for  $\gamma p \rightarrow \Omega^- X$  is simply  $\alpha/\pi$  times the measured hadroproduction rate at ANL [6], which agrees with the above estimates.

The angular distribution of the inclusive and exclusive events may provide clues to the  $\Omega^-$  production mechanism, such as, whether production of  $\Omega(sss)$  is enhanced at small  $t$  or small  $u$  [38].

Brodsky's estimations take an approach to  $\Omega(sss)X$  [38] in which  $g \rightarrow s\bar{s}$  is considered as the origin of one of the  $s$ -quarks. This produces the minimum number of final-state quarks. The other two strange quarks can be made either by gluon splitting  $g \rightarrow s\bar{s}$  or by the double intrinsic strangeness  $|uudss\bar{s}\bar{s}\rangle$  Fock state of the proton. Gluonic intermediate states are expected to be minimized [39]. The  $gs\bar{s}$  vertex produces one of the needed strange quarks. The intrinsic strangeness mechanism does not need explicit gluons. One can create the strange quark pairs within the hadron wave function via QCD Coulomb exchange. This gives the  $|uuds\bar{s}\bar{s}\rangle$  Fock state amplitude. This process is maximally efficient at threshold. The analogous  $|uud\bar{c}\bar{c}\rangle$  double intrinsic charm Fock state can account for the extraordinary  $\pi N \rightarrow (J/\psi)(J/\psi)X$  events seen by the NA3 Collaboration [40] as has been discussed in Ref. [41]. All of the double  $J/\psi$  events are made at high  $x_F(total) > 0.4$ .

Additionally, Shklyar estimated the  $\gamma p \rightarrow \Omega\bar{\Omega}p$  cross section to be picobarns or smaller, which would be hard to measure with sufficient statistics.

## B. Cross Section Estimation for $\Xi$ Photoproduction on the Proton

### 1. Cross Section Estimation of the $\Xi^-(1320)$ Ground State

Due to the lack of data, especially  $\Xi$  photoproduction in exclusive reactions, there has not been much theoretical progress in estimating  $\Xi^{(*)}$  cross sections and understanding their production mechanisms. Recently, however, the production mechanisms were investigated based on an effective Lagrangian approach [15, 42] at the tree level (Fig. 16). Unlike the production of a  $K\bar{K}$  pair, i.e.,  $\gamma N \rightarrow K\bar{K}N$ , where the production via  $\phi$  photoproduction is important, the  $\Xi$  photoproduction process occurs necessarily through the formation of intermediate  $S = -1$  hyperons, namely,  $\gamma N \rightarrow KY \rightarrow KK\Xi$ , since a large contribution from strongly correlated kaon pairs, i.e.,  $S = +2$  exotic mesons, does not seem likely.

In order to reproduce the backward-peaking behavior of the angular distributions for  $\Xi^-$  in the center-of-mass frame (Fig. 17, Right), the high mass hyperons ( $\Lambda(1800)\frac{1}{2}^-$ ,  $\Lambda(1890)\frac{3}{2}^+$ ) must be included in the model, instead of the radiative transitions of the low-mass hyperons.

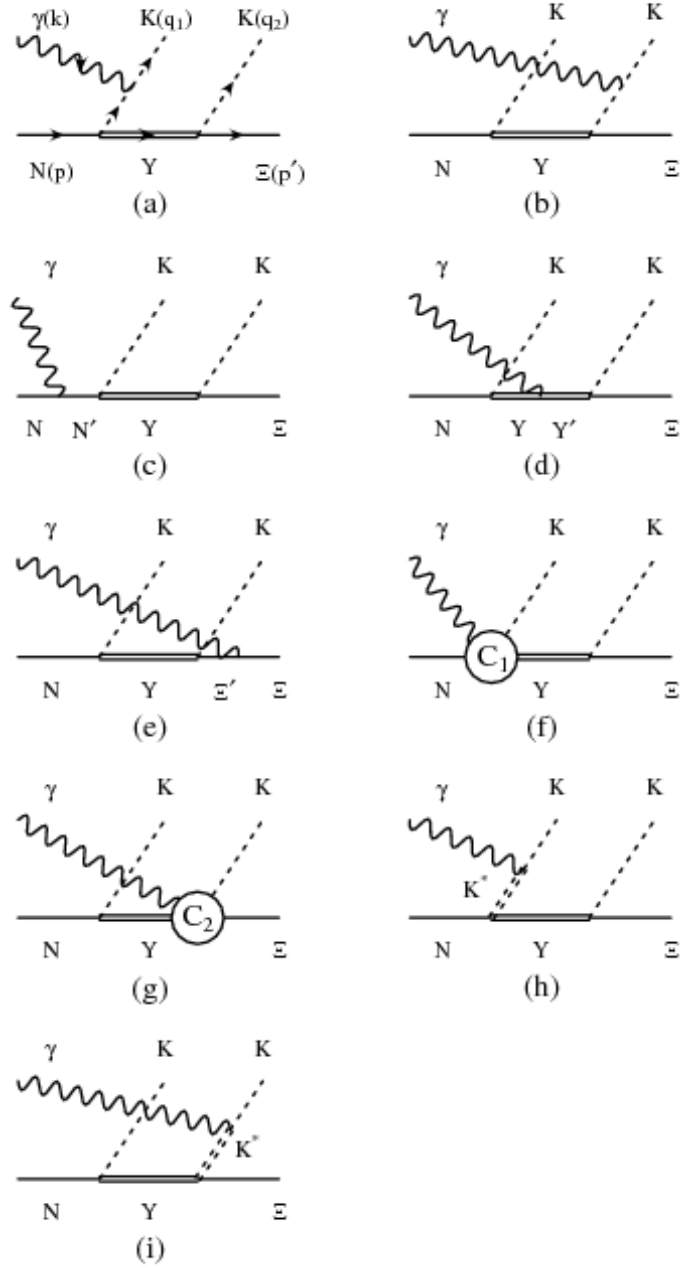


FIG. 16: Diagrams contributing to  $\gamma N \rightarrow KK\Xi$ . The intermediate baryon states are denoted as  $N'$  for the nucleon and  $\Delta$  resonances,  $Y, Y'$  for the hyperon  $\Lambda$  and  $\Sigma$  resonances, and  $\Xi'$  for the  $\Xi(1318)$  and  $\Xi(1530)$ . The intermediate mesons in the  $t$ -channel are  $K$  [(a) and (b)] and  $K^*$  [(h) and (i)]. The diagrams (f) and (g) are the generalized contact currents required to maintain gauge invariance of the total amplitude. The off-shell interaction currents are included in  $C_1$  and  $C_2$ . The diagrams corresponding to (a)–(i) with  $K(q_1) \leftrightarrow K(q_2)$  are also understood.

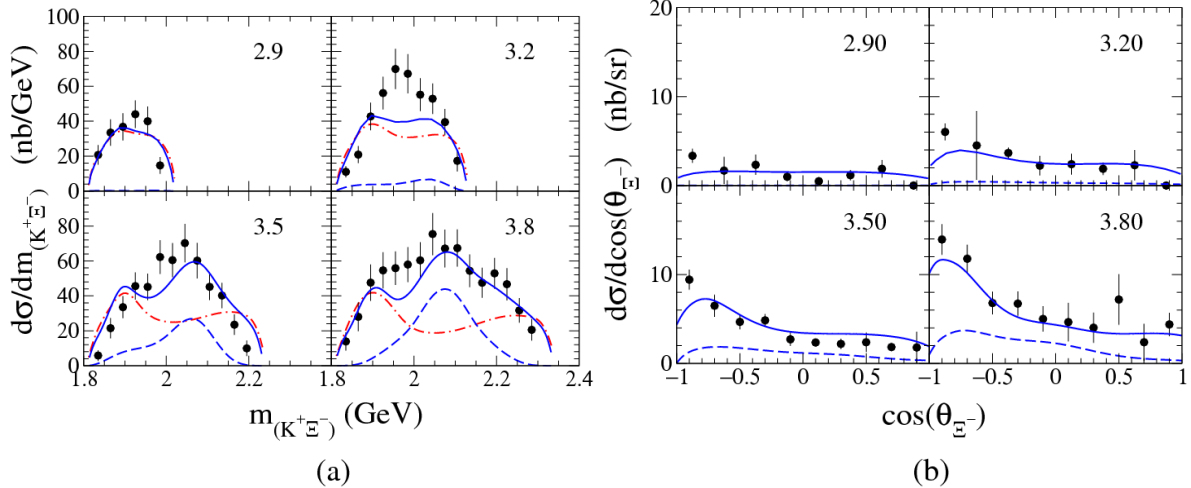


FIG. 17: Comparison of experimental results [14] and theoretical predictions [42]. Left: Invariant mass distribution of the  $K^+\Xi^-$  system in the reaction  $\gamma p \rightarrow K^+K^+\Xi^-$ . Right:  $d\sigma/d\cos(\theta_{\Xi^-})$  results. The number in the right upper corner of each graph indicates the incident photon energy in GeV. The dot-dashed lines are the results of Ref. [15] which includes only spin-1/2 and -3/2 hyperon resonances. The solid lines are the results of the present model, whereas the dashed lines show the contributions from the  $\Sigma(2030)7/2^+$ .

On the other hand, the  $\Sigma(2030)7/2^+$  had to be included to reproduce the  $K^+\Xi^-$  invariant mass spectra (Fig. 17, left). At present, most of the uncertainties in the predicted results arise from the lack of the information on the  $S = -1$  hyperon resonances and their coupling to the  $K\Xi$  channel. By including these high-mass hyperons, the predicted differential cross sections for  $\gamma p \rightarrow K^+K^+\Xi^-$  are consistent with experimental results (Fig. 17). However, due to the overlapping nature of several broad hyperon resonances, it is not necessary for any  $Y^*$  to be directly observed in the  $K^+\Xi^-$  invariant mass spectra. As pointed out in Ref. [15], ground-state  $\Xi$  photoproduction is well-suited for the investigation of the properties of higher-mass  $S = -1$  hyperon resonances.

It is important to note that Ref. [15] predicts a plateauing of the  $\Xi^-(1320)$  cross section at higher photon energies (Fig. 18). However, one needs to keep in mind that only a limited number of higher-mass hyperons are included in the model, while other resonances could also contribute at higher photon energies. It would be interesting to compare these predictions with future CLAS12 results, which could provide more information about whether other higher-mass hyperons need to be included.

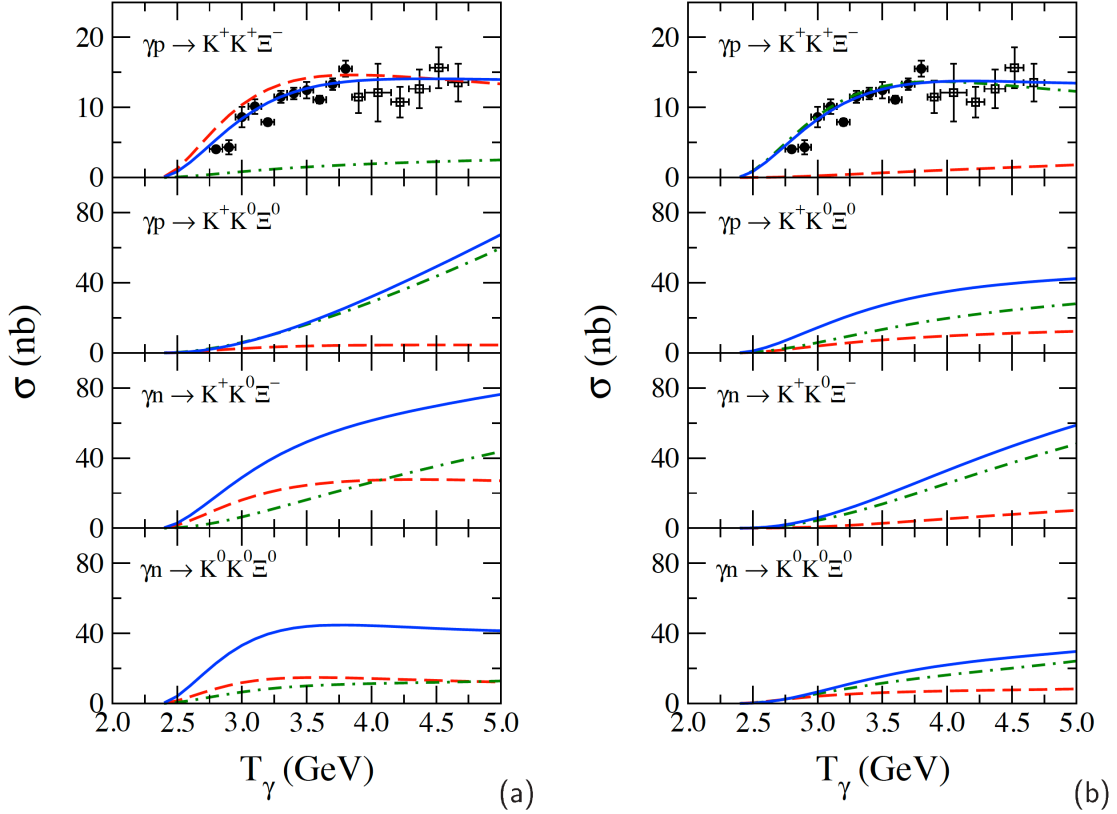


FIG. 18: Total cross sections [15] for  $\gamma N \rightarrow KK\Xi$  according to the mechanisms shown in Fig. 16 as a function of photon incident energy  $T_\gamma$  for (a) pseudovector and (b) pseudoscalar coupling. The dashed curves correspond to the contribution from the diagrams involving only the spin-1/2 hyperons, while the dash-dotted curves correspond to the contribution from the diagrams involving one or more spin-3/2 hyperons. The solid curves represent the total contribution. The data were preliminary and prior to the publication of Ref. [14], where the open boxes are obtained without the differential cross section measurement.

## 2. Cross Section Estimation for the Excited $\Xi$ States

In order to estimate the cross sections for photoproduction of excited  $\Xi$  states, certain assumptions need to be made, mainly due to the lack of information on the coupling of the higher-mass  $Y^*$  states to the excited cascades. Using the quark model predictions of Ref. [43] and only the intermediate  $\Lambda(1116)$  and  $\Sigma(1190)$  hyperon contributions for the  $\Xi^*$  production mechanisms, a rough estimate of the cross sections for excited cascades in the reaction of  $\gamma p \rightarrow K^+ K^+ \Xi^{*-}$  was made by Man et al. [42]. The results (Fig. 19) show that the cross

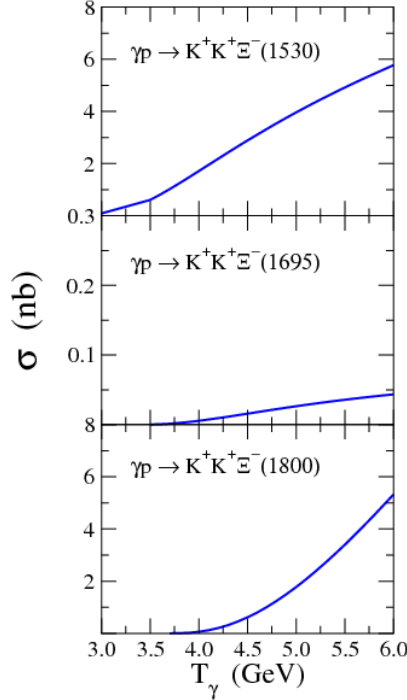


FIG. 19: Predicted total photoproduction cross sections for (top)  $\Xi(1530)_{\frac{3}{2}^+}$ , (middle)  $\Xi(1695)_{\frac{1}{2}^+}$  and (bottom)  $\Xi(1800)_{\frac{3}{2}^-}$ .

sections for the  $\Xi(1530)$ ,  $\Xi(1695)$ , and  $\Xi(1800)$  production are smaller than those for  $\Xi(1318)$  production, as one would expect naturally. In particular, the cross sections for  $\Xi(1695)$  production are smaller than those of  $\Xi(1318)$  production by two orders of magnitude, while this reduction factor is only about 3 for the production of  $\Xi(1530)$  and  $\Xi(1800)$ . In fact, the recent measurements by the CLAS Collaboration reveal much smaller cross sections for  $\Xi(1530)$  photoproduction, by an order of magnitude, than those of  $\Xi(1318)$  photoproduction in the  $K^+K^+\Xi^-$  channel [14]. However, the comparison for  $\Xi(1530)$  and  $\Xi(1320)$  was only possible in a very limited photon beam energy range.

For a more quantitative estimate of these cross sections, it is necessary to include higher-mass  $S = -1$  hyperons as the intermediate states. However, it is important to note that these predictions were made using the same parameters that Ref. [15] used so as to achieve agreement with the experimental data for the  $\Xi^-(1320)$  total cross sections. Therefore, these results should still be useful to estimate the expected rates for producing excited cascades such as the  $\Xi^-(1690)$  and  $\Xi^-(1820)$  at CLAS12.

Clearly, the models described above are just a first step toward building a more complete

and realistic model for describing  $\Xi$  baryon photoproduction off nucleons. The CLAS results have already played an important role in the development of these models. In order to pin down the production mechanism of  $\Xi$  baryons and to uncover the role of the higher-mass  $S = -1$  hyperons, it is clear that future CLAS12 results will be extremely useful.

## V. SPECIALIZED DETECTOR COMPONENTS

In this section we outline the specialized detector components relevant to the proposed experiment, in addition to the standard CLAS12 equipments.

### A. Forward Tagger

The forward tagger (FT) equipment will characterize and identify quasi-real photons via measurement of electrons scattered at small-angles. The FT will provide electron detection for the region  $2.5^\circ < \theta_{e'} < 4.5^\circ$ , which is outside of the acceptance region of the CLAS12 detector. The FT comprises a *calorimeter* (FT-Cal), to identify the scattered electron, measure the electromagnetic shower energy and provide a fast trigger signal; a *tracker* (FT-Trck) to provide accurate measurements of the scattering angles ( $\tan \theta_{e'}$  and  $\phi_{e'}$ ); and a *scintillation hodoscope* (FT-Hodo) to provide high efficiency  $e/\gamma$  separation. A dedicated trigger system will provide a fast signal to identify a timing coincidence with signals from CLAS12.

The three components of the FT will be placed between the High Threshold Cerenkov Counter (HTCC) and the torus support, at about 190 cm downstream of the target (nominal) position. Figure 20 shows a CAD drawing of the FT elements integrated in CLAS12.

Table IV gives the kinematic ranges of the FT system. The energy range of tagged photons is extended from the nominal value of 6.5-10.5 GeV to include the  $\Omega^-$  threshold. This is within the expected operating range of the device.

### B. The Calorimeter: FT-Cal

The geometrical size of the calorimeter is determined by the need for coverage in close proximity to the beam line ( $2.5^\circ$  corresponds to  $\sim 8$  cm) and the limited space available in

	<i>Range</i>
$E_{e'}$	0.5 - 6.0 GeV
$\theta_{e'}$	$2.5^\circ$ - $4.5^\circ$
$\phi_{e'}$	$0^\circ$ - $360^\circ$
$E_\gamma$	5.0 - 10.5 GeV
$P_\gamma$	75 - 100%
$Q^2$	0.01 - 0.3 GeV <sup>2</sup> ( $< Q^2 > 0.1$ GeV <sup>2</sup> )
W	3.2 - 4.5 GeV

TABLE IV: Kinematic range of the FT.

this region (at most  $\sim 40$  cm along the beam axis). This requires a compact calorimeter with a material having short radiation length. The size of each calorimeter pixel should be comparable with the characteristic transverse size of the electromagnetic shower or Moliere radius, so as to limit the signal induced by an incident electron to a few pixels, thus minimizing pixel rates and pile-up. The FT-Cal will be based on homogeneous PbWO<sub>4</sub> crystals, arranged in an array of 408 crystals of size  $15 \times 15 \times 200$  mm<sup>3</sup>. In recent years materials such as PbWO<sub>4</sub> have been extensively studied and shown to be very resistant to radiation damage, which can be significant in this region close to the beam line. The PbWO<sub>4</sub> has a very fast scintillation decay time (6.5 ns), a very small radiation length (0.9 cm) and small Moliere radius (2.1 cm). With this design an energy resolution of  $(2\%/\sqrt{E(\text{GeV})} \oplus 1\%)$  is expected. The electron energy resolution is a crucial factor to determine precisely the photon energy and to ensure the exclusivity of the measured reaction via missing-mass techniques. However, since we are interested in low-energy electrons and high-energy photons, the energy resolution for the latter will be significantly better than for the former.

### C. The Scintillation Hodoscope: FT-Hodo

The primary aim of the hodoscope for the forward tagger is to discriminate between photons and electrons that produce an electromagnetic shower in the calorimeter. The scintillation hodoscope, placed in front of the calorimeter, will be made of 2 layers of Eljen EJ-204 plastic scintillator tiles read-out by Hamamtsu  $3 \times 3$  mm<sup>2</sup> silicon photomultipliers

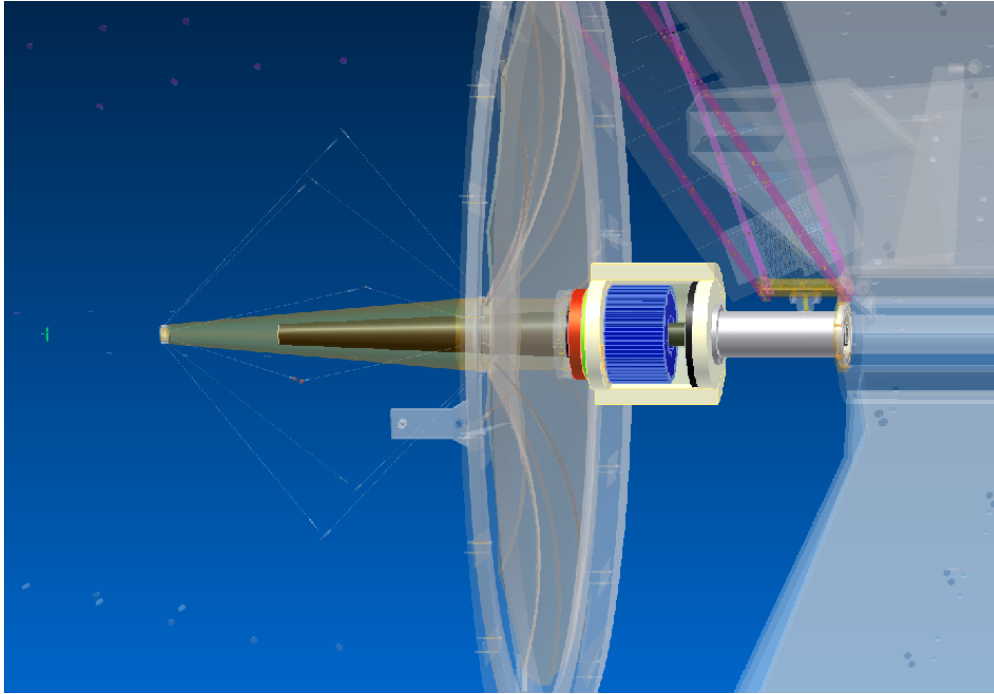


FIG. 20: CAD drawing showing the integration of the FT in CLAS12. The FT is located in the free space between the HTCC and the first DC layer. The calorimeter (FT-Cal) shown in blue is located at about 190 cm from the interaction point, shown by the green cross, and is enclosed in a Rohacell case to provide thermal insulation. The FT-Hodo (green) and the first tracker layer of FT-Trac (red) are located in front of the calorimeter. A tungsten cone (black) shields the FT from Møller electrons and electromagnetic background created by the beam.

(S10362-11-100C) via  $\sim 4$  wavelength shifting fibers per hodoscope tile. Each hodoscope plane will be segmented into around 120 elements, most of which have a pixel size corresponding to 4 calorimeter crystals. The inner ring comprises tiles having the dimension of a single calorimeter crystal. The double layer design of FT-Hodo reduces to less than 1% the splashback of charged particles produced by photons in the calorimeter, which could result in particle misidentification due to false-firing hodoscope elements. The hodoscope layers comprise 7 mm and 15 mm thick scintillator tiles, with the latter layer designed to give sub nanosecond timing resolution for the particle. The requirement of a coincident hit between the layers will also reduce contributions of false events from SiPMT noise. The wavelength shifting fibers will be fusion spliced to an optical fiber having about a 15 m attenuation length. The fibers will connect to the SiPMTs away from CLAS12 in a radiation-safe region.

#### **D. FT-Trck**

The role of the tracker is to provide a reconstruction of the charged-particle track, essentially from electrons, with polar angles between  $2.5^\circ$  and  $4.5^\circ$ . In this forward-angle region the background count rate can be several hundreds of kHz/mm<sup>2</sup>, requiring a highly segmented high-rate tracking system. FT-Trck will comprise two double layers of micromegas detectors located in the space between the calorimeter and the High Threshold Cherenkov Counter (HTCC). The detectors will be annular-shaped with inner and outer radii of 65 mm and 160 mm, respectively. The use of two micromegas layers is a compromise to achieve an efficient background rejection and track reconstruction with a low material budget. These two layers are each composed of two single micromegas with perpendicular strips, enabling the (X,Y) coordinates of a track to be determined. The pitch is 500  $\mu\text{m}$ , which leads to a spatial resolution better than  $500/\sqrt{12} = 144 \mu\text{m}$ . Angular resolutions for electrons of  $\sim 1.7\%$  and  $2.8^\circ$  in  $\theta$  and  $\phi$  are expected.

The FT readout will follow the scheme adopted for the Micromegas-based on central tracker detectors. The front-end electronics will provide pre-amplification and shaping of the detector signals, pipeline buffering during the trigger generation process, digitization and compression of selected event data. This is then delivered to the back-end electronics which will pack the data and interface with the CLAS12 event building system. The readout comprises about 5k electronics channels which can handle hit rates of up to 100 kHz per

channel.

### **E. Trigger**

The reactions of interest in the proposed experiment have several charged final state particles, therefore our trigger requires a minimum of two tracks. This is consistent with the exotic-meson proposal's two track trigger, in coincidence with the forward tagger [48], and can run parasitically in this respect.

### **F. Present Status of the FT Project**

The forward tagger system is being designed and built by a collaboration of several institutions including, the Italian National Institute for Nuclear Physics (INFN), the French Commissariat l'Energie Atomique (CEA), the University of Edinburgh, James Madison University, Norfolk State University, the University of Ohio, and Jefferson Lab. Funds for the construction of the FT-Cal will be provided by INFN, while funds for the construction of the FT-Hodo and FT-Trck were requested via an MRI that was submitted to NSF in January 2012. Additional financial contributions will be provided by Jefferson Lab, the University of Edinburgh and by the European Commission via the FP7-HP3 project.

The conceptual design of the detector has been fully developed, and R&D on the different components has been in progress for more than two years with the aim of finalizing the detector technical design and starting the construction phase within 2012. To validate the proposed design of the FT-Cal and FT-Hodo, prototypes were built and installed in Hall B for a test run with the electron beam in December 2011. The FT-Cal prototype consisted of a  $3\times 3$  matrix of PbWO crystals, read-out with  $10\times 10$  mm<sup>2</sup> LAAPDs by Hamamatsu. The mechanical structure to support and thermally stabilize the crystals, as well as the front-end electronics, was based on the layout developed for the full FT-Cal. The hodoscope prototypes consisted of plastic scintillator tiles of various sizes and thickness, connected to different numbers of WLS fibers for the light collection. The fibers were coupled to the Hamamatsu  $3\times 3$  mm<sup>2</sup> SIPM that was selected for this detector system. The SIPM signal was amplified with a preamplifier prototype and readout with the same front-end electronics used for the calorimeter prototype. The FT-Hodo prototype was installed in front of the

FT-Cal prototype to intercept the trajectories of electrons hitting the central crystal of the calorimeter matrix. The test data are presently being analyzed but initial results showed that the observed signals from both prototypes are consistent with the expectations. Preliminary estimate of the FT-Cal prototype energy response indicated a resolution below 3% can be achieved for an electron energy of  $\sim 1.2$  GeV. Further tests of improved FT-Cal and FT-Hodo prototypes are planned at the LNF Beam Test Facility [49] in May 2012. These new measurements will allow us to determine the energy and time resolution, and test the calibration procedures for both systems. R&D on the FT-Trck is in progress at CEA-Saclay in conjunction with the development of the micromegas tracker for the CLAS12 Central Detector. The layout and structure of these detectors are very similar and will allow us to exploit the experience gained in the development of the central detector tracker in defining the layout of the FT tracker. The first tests on the micromegas prototypes were completed, showing that the mechanical characteristics are within specifications and that the measured gain and response to cosmic rays are consistent with expectations.

## VI. CLAS12 MEASUREMENT FOR THE $\Omega^-$ AND $\Xi^{(*)}$ BARYONS

In order to observe the  $\Omega^-$  and high mass  $\Xi$  states for the first time in photoproduction, the experiment needs high luminosity combined with large acceptance and a beam energy extending well above threshold. These conditions can all be met at CLAS12.

To estimate the number of  $\Omega^-$  and cascades produced, we take the nominal CLAS12 luminosity of  $10^{35}$  cm<sup>2</sup>s<sup>-1</sup>. We consider 3 possibilities for the production photon in the energy range 5-11 GeV; (a) a real bremsstrahlung photon from the  $e^-$  beam in the liquid hydrogen target, (b) a quasi-real photon tagged in the forward tagger (FT), and (c) an untagged quasi-real photon, i.e. the low angle scattered  $e^-$  not in the FT acceptance. Cases (a) and (c) will be experimentally indistinguishable.

The flux of real bremsstrahlung photons has been estimated using two methods; first through evaluating Equation 27.28 in the PDG book, giving the number of photons per electron,

$$n_\gamma = \frac{d}{X_0} \left[ \frac{4}{3} \ln \left( \frac{k_{max}}{k_{min}} \right) - \frac{4(k_{max} - k_{min})}{3E} + \frac{k_{max}^2 - k_{min}^2}{2E^2} \right]$$

, with  $d = L\rho = 5$  cm  $\times 0.0708$  g cm<sup>-3</sup>.  $X_0 = 63$  g cm<sup>-2</sup> is estimated from two different PDG equations, (27.22) and (27.24) [1]. For  $k_{max} = 11$  GeV and  $k_{min} = 5$  GeV,  $n_\gamma = 0.0040$ .

The second method used a GEANT4 simulation of 11 GeV  $e^-$  incident on a 5 cm thick liquid hydrogen target. The number of photons leaving the target per  $e^-$  was found to be 0.0048, in reasonable agreement with the calculation. Production estimates for this case will use the lower calculated figure of 0.0040. To calculate the photon luminosity, we take  $L_\gamma = L_e \times \frac{n_\gamma}{2} = 2 \times 10^{32} \text{ cm}^2\text{s}^{-1}$ , where the factor 2 in the denominator accounts for an effective target length (*i.e.*, half the length of the target cell).

The flux of tagged and untagged quasi-real photons has been calculated via the RADGEN1.0 program [44], which accounts for internal radiative corrections to the cross section. For both cases the scattered electron energy is integrated from 0.5 to 6 GeV, while for the tagged case the scattering angle is integrated from 2.5 to 4.5°. The resulting luminosities are  $L_{\gamma*tag} = 8.7 \times 10^{31} \text{ cm}^2\text{s}^{-1}$  for tagged and  $L_{\gamma*unt} = 3.2 \times 10^{32} \text{ cm}^2\text{s}^{-1}$  for untagged.

We therefore expect that most baryons will be produced by untagged quasi-real photons with a further 63% from untagged bremsstrahlung and 27% from tagged quasi-real photons. Baryons from the two former mechanisms will have to be fully reconstructed with any associated particles to fully determine the reaction. On the other hand, with tagged quasi-real photons, it is possible to measure incomplete final states and use the missing mass to determine the reaction. Using such a method can substantially increase the reaction acceptance.

### A. Measurements of $\Omega^-$ Production

The feasibility of cross section measurements for  $\Omega^-$  photoproduction has been investigated with CLAS12 parameterized Monte Carlo simulation FASTMC.

The relevant production and decay chain for  $\Omega^-$  production is,

$$\begin{aligned}
 \gamma p &\rightarrow K^+ K^+ K^0 \Omega^- \\
 K^0 &\rightarrow \pi^+ \pi^- \quad (BR = 34\%) \\
 \Omega^- &\rightarrow K^- \Lambda \quad (BR = 68\%) \\
 &\rightarrow \pi^- \Xi^0 (\pi^0 \Lambda) \quad (BR = 24\%) \\
 \Lambda &\rightarrow p \pi^- \quad (BR = 64\%)
 \end{aligned}$$

To fully measure the final state requires detection of 7 particles;  $2K^+$ ,  $\pi^+$ ,  $\pi^-$  from  $K^0$  decay,  $K^-$  from  $\Omega^-$  decay and the proton and  $\pi^-$  from the  $\Lambda$  decay. If the production photon is tagged then, in principle, it is possible to identify the  $\Omega^-$  events by measuring the 3 associated kaons (with the  $\pi^+\pi^-$  for the  $K^0$ ), this is then sufficient to fully reconstruct the reaction. Further measurement of the  $\Omega^-$ ,  $K^-$  or  $\pi^-$ , allows reconstruction of the  $\Omega^-$  decay and provides a means of background rejection.

In addition to the standard FASTMC reconstruction, an additional constraint has been placed on the vertex position of the measured particles. Many of the intermediate particles can travel significant distances in the detector before decaying, and some particles may be created outside of the vertex detector. It is assumed for this analysis that such particles will not be reconstructed. This is erring on the side of caution as in reality such particles can be reconstructed, albeit with degraded momentum resolution. A particle was considered to be detected inside the vertex detector if its vertex distance from the center of the target was less than 5 cm transverse and 19 cm longitudinal. Such constraints result in reconstruction losses of 10% ( $K^-$ ), 23% ( $K^0$ ) and 50% ( $\Lambda$ ). These losses are accounted for in the event rate estimates in Table 4.

The  $\pi^-$  from the  $\Lambda$  decay suffered from particularly poor acceptance, due to its low momentum, forward angle and inward trajectory. This subsequently leads to a poor acceptance for the detection of all 7 particles in the final state.

We consider four different final state topologies; (i) Detect  $2K^+$ ,  $\pi^+$ ,  $\pi^-$ , (ii) same as (i) adding a  $K^-$ , and cutting on the reconstructed mass of the  $\Lambda$ , (iii) same as (i) adding a  $\pi^-$  and cutting on the reconstructed mass of the  $\Xi^0$ , and (iv) detect all 7 final state particles from  $K^-\Lambda$  decay. The production acceptances are shown in Fig. 21 as a function of beam energy.

The additional kinematic and vertex cuts placed during the analysis were: (i) for  $K^0$  detection, the  $\pi^+$  and  $\pi^-$  were required to have the same vertex and reconstruct the mass of the  $K^0$  within  $4\sigma$ , (20 MeV); (ii) for the case of a missing  $\Lambda$ , the missing mass had to be within  $4\sigma$ , (120 MeV) of the  $\Lambda$  mass; the  $K^-$  vertex position had to be greater than 2 mm from the  $K^+$  vertex, and (iii) For the missing  $\Xi^0$  a  $3\sigma$  cut was placed on the missing mass and the  $\pi^-$  vertex had to be greater than 2 mm from the  $K^+$  vertex.

Although a RICH detector would certainly help the kaon identification, it is not absolutely necessary for the detection of  $\Omega^-$ . Due to the presence of many final state particles in

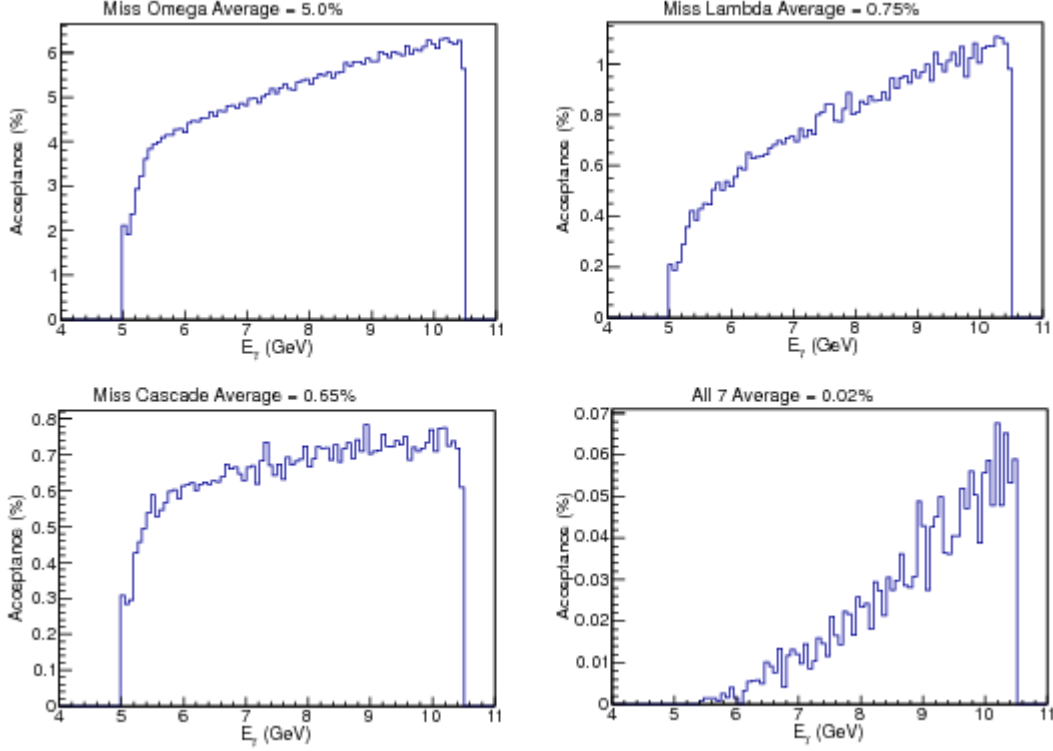


FIG. 21: The acceptance for phase-space  $\Omega^-$  detection as a function of photon beam energy. Top left requires detection of  $2K^+$ ,  $\pi^+$ ,  $\pi^-$ ; top right, an additional  $K^-$ ; bottom left, an additional  $\pi^-$  from  $\Omega^-$  decay to  $\Xi^0\pi^-$ ; and bottom right detection of all 7 charged particles in the  $K^-\Lambda$  channel.

$\Omega^-$  production, the momentum range for the kaons are typically well within the kinematic regions where  $K/\pi$  separation is excellent. For all the final state particles in the reaction  $\gamma p \rightarrow K^+K^+K^0\Omega^-$ , the distributions of  $\beta$  as a function of their momenta are shown in Fig. 22, based on the simulation discussed above. Clearly, the majority of the kaons have momentum less than 2 GeV.

### 1. Event Rates for $\Omega^-$ Photoproduction

We can now calculate the expected event rates for these four possibilities. We assume a photoproduction cross section of 0.3 nb, from Fig. 15, a tagged luminosity of  $8.7 \times 10^{31} \text{ cm}^2\text{s}^{-1}$ , and untagged luminosity  $5.2 \times 10^{32} \text{ cm}^2\text{s}^{-1}$ . Table 4 shows the detection efficiencies, production rates and measured events per hour for the CLAS12 detector, operating at half toroidal field strength, with an electron beam luminosity of  $10^{32} \text{ cm}^2\text{s}^{-1}$ .

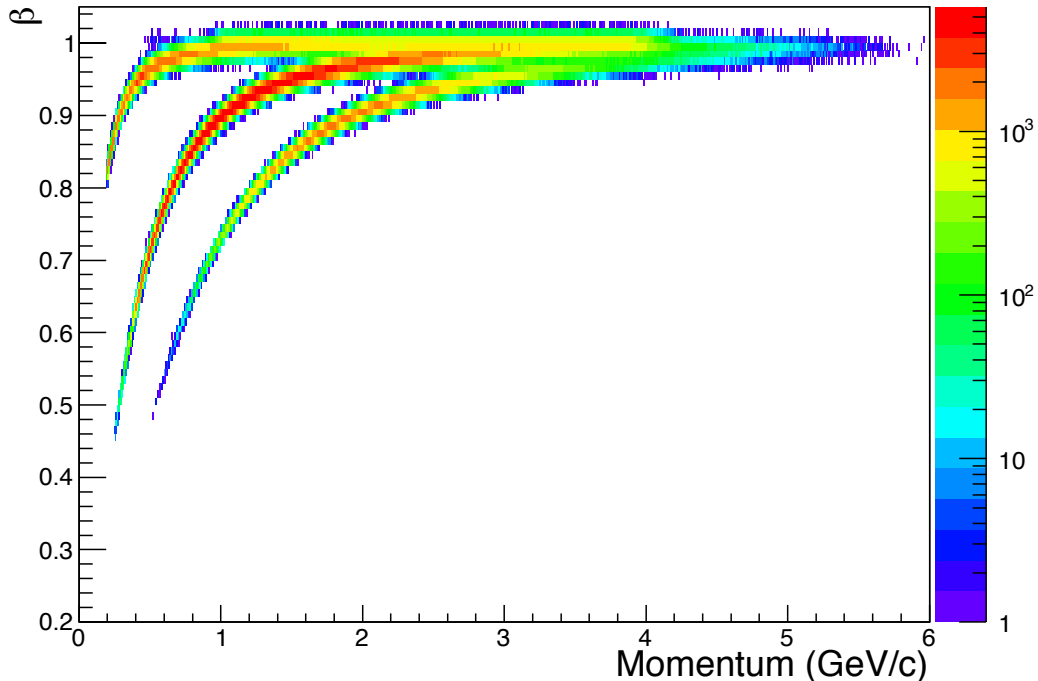


FIG. 22: Simulated distributions of  $\beta$  as a function of momentum for all the final state particles in the reaction  $\gamma p \rightarrow K^+ K^+ K^0 \Omega^-$ .

The highest possible event rate will come from detecting the 3 associated kaons, observing an electron in the Forward Tagger, and reconstructing the  $\Omega^-$ . In 80 days of beam time, this would provide 6.9k  $\Omega^-$ 's integrated over all energies and angles.

Estimates of the contributions of background processes, outlined in Sec.VIA 2, are very high for this  $3K$  topology (approximately 1:10, signal to background). In this case, detecting part of the  $\Omega^-$  decay in addition appears to be the more appealing method. We can measure either the  $K^-$  or the  $\pi^-$  from decays to  $\Lambda K^-$  and  $\Xi^0 \pi^-$ , respectively. The latter has a more uniform acceptance over all beam energies, whereas the former has a higher overall efficiency as shown in Fig. 21. We estimate that in 80 days we will obtain 1k and 0.8k events for the additional  $K^-$  and  $\pi^-$ . This would provide around 75 events per 250 MeV photon beam energy bin.

Detecting the full final state will lead to only around 75 events in total but will provide a useful systematic check of the acceptances.

Detected	Det. Eff. (%)	Vertex Eff.	Prod. Rate (1/h)	Measured Events (1/h)
$K^+K^+K^0$	5.0	77	94	3.6
$K^+K^+K^0K^-$	0.75	70	94	0.5
$K^+K^+K^0\pi^-(\Xi^0)$	0.65	70	94	0.4
All 7	0.02	35	561	0.04

TABLE V: Event rate estimates for 4 different scenarios. The measured events are the product of the detection efficiency, vertex efficiency and production rate.

## 2. Background

In principle, measuring a reaction with a relatively low cross section and large multiplicity in the final state is a daunting task as large backgrounds from other physics processes can overwhelm the signal of interest. However,  $\Omega^-$  photoproduction has a number of signatures that can help reduce the hadronic background. It is produced in association with 3 kaons, it has a decay vertex, detached from the production vertex and one of the decay product ( $\Lambda$ ) has a detached vertex. To estimate the backgrounds contributing to the the various final states an event generator based on Pythia was used [45]. The hadronic background produced was then normalized to the expected cross section for  $\Omega^-$  photoproduction of 3 nb. As the number of hadronic events produced over 100 days is on the order of  $10^{11}$ , the resulting histograms from  $2 \times 10^8$  simulated events had to be scaled up significantly.

The results for just 3 detected kaons are shown in Fig. 23. We see a considerable background as expected in this case, which yields a signal to background ratio of around 1:10 in the peak region. It may be possible to significantly reduce this background by investigating other detected particles, but this has not yet been attempted.

If we now require a  $K^-$  in coincidence, the situation is improved. First cutting on the missing mass around the  $\Lambda$  reduces the signal to background ratio to around 1:2. In addition, if a cut on the vertex difference for the  $K^-$  and  $K^+$  of greater than 2 mm is applied (expected resolution is around 0.5 mm) then zero background events survive, giving a clean signal, see Fig. 24 (left). A similar situation is found when detecting an additional  $\pi^-$  from the decay to  $\Xi^0\pi^-$ , although in this case the final background may not be zero, but is expected to be lower than the signal.

The fact that we can reconstruct the  $\Omega^-$  signals with virtually zero background should

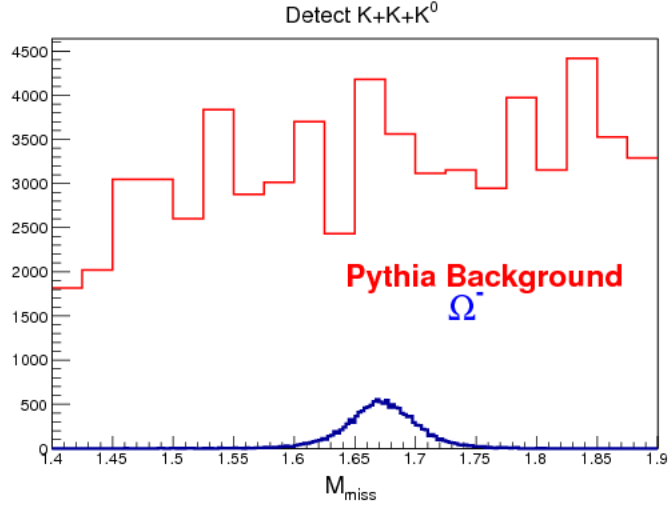


FIG. 23: The expected event distribution for  $\Omega^-$  photoproduction, blue, and Pythia background, red.

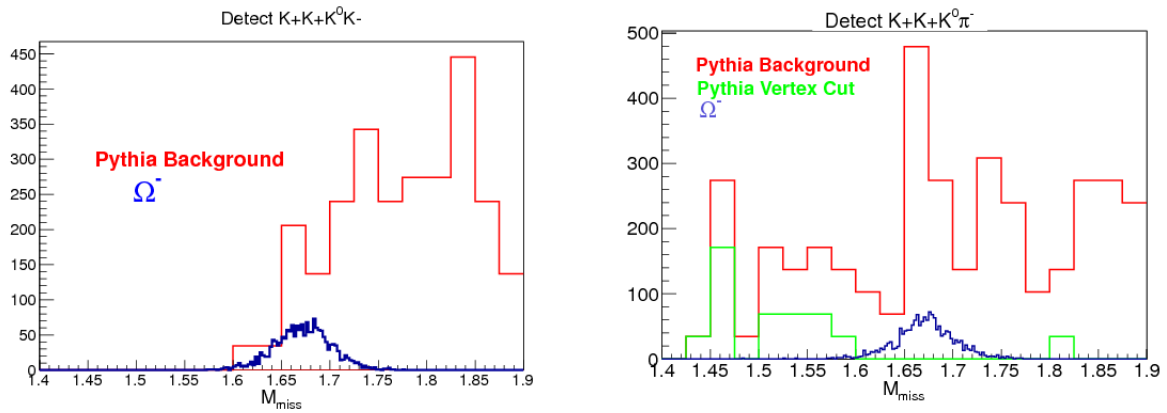


FIG. 24: The expected event distribution for  $\Omega^-$  photoproduction, blue, Pythia background, red, and Pythia background with a vertex cut, green. Note, in the right plot the vertex cut removes all Pythia background.

be no surprise, due to the double kinematic constraint of the 3-kaon's missing particle being the  $\Omega^-$ , and the 4-kaon's missing particles being the  $\Lambda$ , in addition to the vertex cuts. In fact, such a clean signal have already been demonstrated in CLAS when the  $\Xi^-(1320)$  is studied (Fig. 7), even without a vertex detector.

## B. Measurements of $\Xi^{(*)}$ Production

Similarly, the production of the established  $\Xi^-$  states such as the  $\Xi^-(1320)$  and  $\Xi^-(1530)$  has been studied via extensive simulation. In the case of the ground state  $\Xi^-$ , although it can be reconstructed directly via the reaction  $\gamma p \rightarrow K^+ K^+(X)$ , it is necessary to detect the decay product in order to extract the polarization observables. The overall detection efficiency for the reaction  $\gamma p \rightarrow K^+ K^+ \pi^-(\Lambda)$  is 9.3%. Assuming a cross section of 15 nb in the CLAS12 energy range, we expect a total number of 0.9 M  $\Xi^-$  events with the decay product detected. This represents two orders of magnitude more statistics than existing CLAS data. In the case of the  $\Xi^-(1530)$ , it can be investigated in the reaction  $\gamma p \rightarrow K^+ K^+ \pi^-(\Xi^0)$ . The overall detection efficiency has been determined to be 7.4% from simulation. Assuming a cross section of 6 nb, the total number of  $\Xi^-(1530)$  events will exceed a quarter million.

## C. Determination of the Spin-Parity of the Excited Cascades

In the existing CLAS data are limited by the beam energy, and the very low cross sections of cascade resonances other than the  $\Xi(1320)$  and  $\Xi(1530)$  makes it very difficult to observe them. Even if small signals of some of these higher states are observed, it is unlikely that there will be enough statistics for a spin and parity measurement. In CLAS12, however, due to the higher energy and expected higher cross sections at these energies for the excited cascade resonances, it is predicted and expected that enough statistics can be collected so that the spin and parity of the produced states can be either confirmed or measured directly for the first time.

In order to determine spin and parity of an excited cascade, the so called Double Moment Analysis (DMA) can be employed [46, 47]. If only  $\Xi^{*-} \rightarrow \Lambda(\frac{1}{2}^+) \pi^-(0^-)$  is reconstructed, then due to the Minami ambiguity, there could be two solutions for  $J^{\pm P}$ . In order to solve the problem, one needs to detect the decay of the daughter hyperon as well, for example,  $\Lambda \rightarrow p \pi^-$ . If there are sufficient statistics, then the double moments can be analyzed to determine the  $J^P$  assignment of the parent cascade. The double moments, typically denoted by  $H(lmLM)$ , are defined by:

$$H(lmLM) = \Sigma D_{Mm}^L(\theta_1, \phi_1) D_{m0}^l(\theta_2, \phi_2), \quad (10)$$

with  $(\theta_1, \phi_1)$  being the decay angles of the  $\Xi^*$ , and  $(\theta_2, \phi_2)$  being the decay angles of the

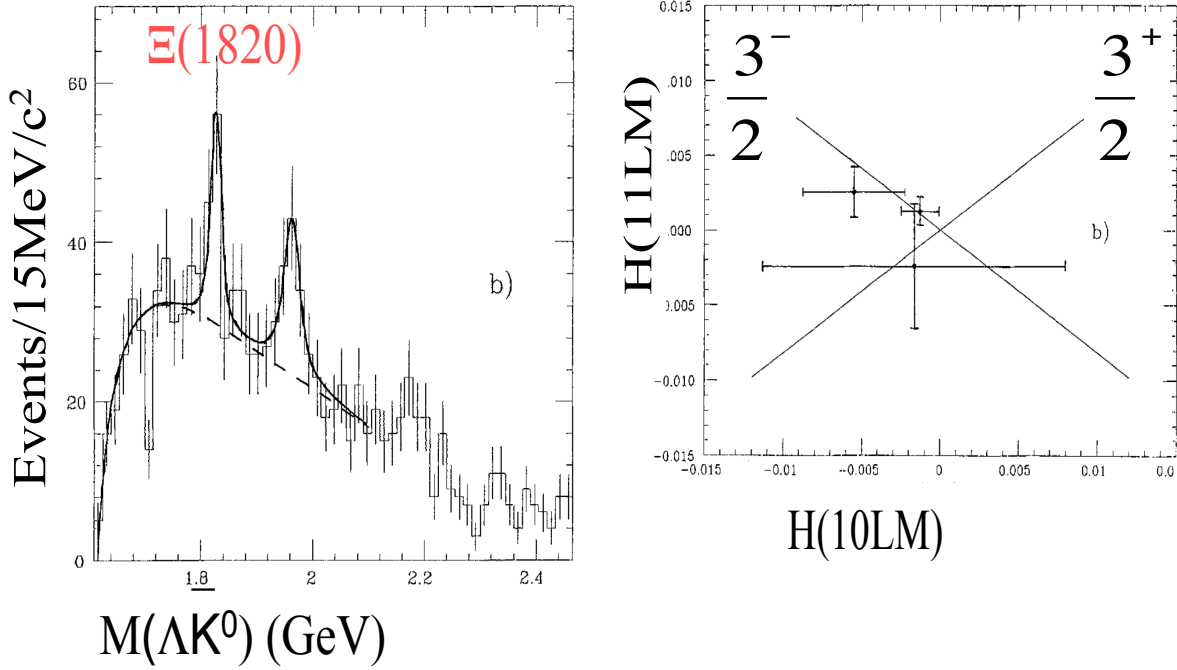


FIG. 25: Left: Invariant mass spectrum of  $\Lambda\bar{K}^0$  in the inclusive  $\Xi - Be$  reaction [46]; Right: The  $H(11LM)$  moment vs. the  $H(10LM)$  moment for the  $\Xi(1820)$  signal region.

$\Lambda$ . The DMA technique takes advantage of the linear dependence between different double moments, given by

$$H(11LM) = P(-1)^{J+\frac{1}{2}} \frac{2J+1}{\sqrt{2L(L+1)}} H(10LM). \quad (11)$$

This linear dependence gives simple and multiple tests for the  $J^P$  assignment for combinations of any odd  $L \leq 2J$  and  $M \leq L$ , therefore providing reliable measurements of the quantum numbers of the excited cascades. In fact, this is how the  $J^P$  of the  $\Xi(1820)$  state was determined (Fig. 25) using only 50 signal events [46]. In order to perform such an analysis, it is necessary to reconstruct the whole decay chain such as  $\Xi^{*-} \rightarrow \Lambda K^-$ ,  $\Lambda \rightarrow p\pi^-$ .

There already exist CLAS data for the reaction of  $\gamma p \rightarrow K^+ K^+ K^- (\Lambda/\Sigma)$  that are needed to detect states such as  $\Xi^-(1820)$ . The  $g12$  experiment, in fact, does show clean signals of  $\Lambda$  and  $\Sigma$  (Fig. 26) in the missing mass of the  $(K^+ K^+ K^-)$  system. However, assuming 20% of these  $\Lambda$  events are from the  $\Xi^-(1820)$  decay, taking into account that the  $\Lambda$  decays into  $p\pi^-$  only 64% of the time, and that the branching ratio of  $\Xi^-(1820)$  decaying into  $\Lambda K^-$  is about 30%, the number of detectable  $\Xi^-(1820)$ 's will dramatically decrease. Since the proton acceptance at CLAS is generally below 50% in the  $g12$  experiment, there would not

have been more than 20 events of  $\Xi^-(1820)$  in  $g12$  with the whole decay chain reconstructed. The implication is that, in order to measure the  $J^P$  of excited cascades, one need to conduct the experiment at as high an energy as possible, in order to reach the region where the cross section is sizable, to compensate for the inefficiency of detecting multiple final state particles.

Based on the projected CLAS12 luminosity, with the lower end of the predicted cross section (Ref. [15]) of 3 nb, and the overall detection efficiency of 0.63% based on simulation (including the branching ratios), the rate of  $\Xi^-(1820)$  observation is estimated at 6 per hour. If 80 days of beam time are used, then more than ten thousand  $\Xi^-(1820)$  events can be observed with the whole decay chain reconstructed, two orders of magnitude more than existing data. Data on other higher mass states would almost certainly amount to discoveries, since the  $\Xi^-(1820)$  is the highest-mass state with both spin and parity determined.

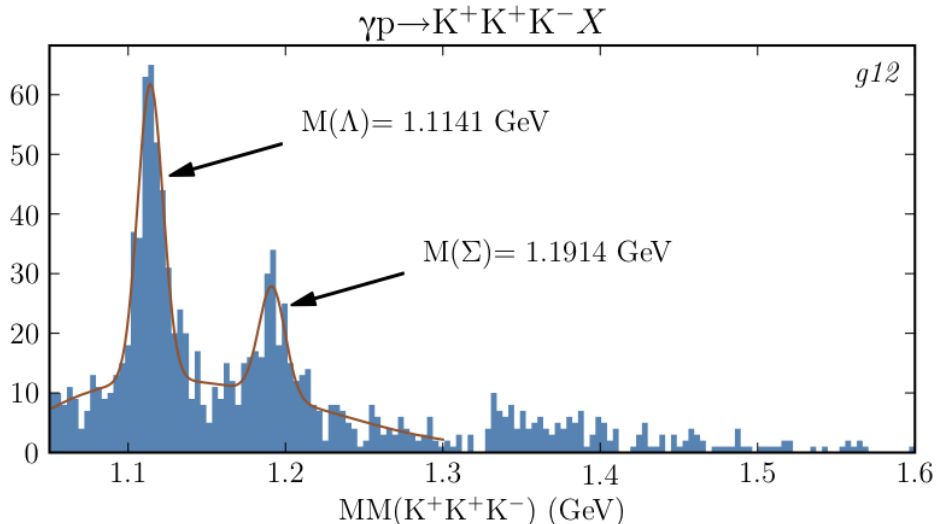


FIG. 26: Missing mass distribution off the  $K^+ K^+ K^-$  system in the reaction of  $\gamma p \rightarrow K^+ K^+ K^- (X)$  from the  $g12$  experiment. The maximum photon energy is 5.4 GeV.

## VII. BEAM TIME REQUEST AND EXPECTED RESULTS

The proposed experiment would run concurrently with the approved meson spectroscopy experiment (E12-11-005) at CLAS12. The approved beam time for the experiment E12-11-005 is 80 days, sufficient to collect enough statistics and achieve all of our major goals. Using

the predicted cross section results and the simulation results as discussed in the previous sections of this proposal, the expected total number of events for a few benchmark reactions are summarized in Table. VII.

State	Detected Particles	Measured decays	Overall Efficiency	Observed Rate/hr	Total detected
$\Omega^-$	$K^+K^+K^0(\Omega^-)$		3.85%	3.6	7k
$\Omega^-$	$K^+K^+K^0K^-(\Lambda)$	$\Omega^-$	0.53%	0.5	1k
$\Xi^-$	$K^+K^+\pi^-(\Lambda)$	$\Xi^-$	9.3%	440	0.9M
$\Xi^-(1530)$	$K^+K^+\pi^-(\Xi^0)$	$\Xi^-(1530)$	7.4%	140	270k
$\Xi^-(1820)$	$K^+K^+K^-\pi^-(\pi^-)$	$\Xi^-(1820), \Lambda$	0.63%	6	12k

TABLE VI: Expected particle rates with the approved 80 beam time for the experiment E12-11-005. The cross sections used in the estimate are 0.3 nb for  $\Omega^-$ , 15 nb for  $\Xi^-$ , 6 nb for  $\Xi^-(1530)$ , and 3 nb for  $\Xi^-(1820)$ . The various decay branching ratios were taken into account. (The branching ratio of  $\frac{\Gamma(\Lambda\bar{K})}{\Gamma_{total}}$  is assumed to be 0.3)

Clearly, the expected total number of  $\Omega^-$  events in  $\gamma p \rightarrow K^+K^+K^0(\Omega^-)$  would be sufficient to perform differential cross section measurements. Based on the simulation we have conducted, the projected  $\Omega^-$  counts as a function of  $E_\gamma$  and  $\cos\theta_{c.m.}^{\Omega^-}$  are shown in Fig. 27(left), with the  $\Omega^-$  detected from the missing mass of the three kaon system. The uncertainty of the total cross sections as a function of  $E_\gamma$  is shown in Fig. 27(right), including only the statistical uncertainty and assuming the cross section is constant at 0.3 nb. Although the statistics will decrease if  $K^-$  is also required, but it still will be sufficient as a systematic check against the three-kaon topology. Most importantly, this channel will be virtually background free(Fig. 24, right).

The relations between the cascade and beam polarizations and other kinematic variables can be studied in the almost one million  $\Xi^-$  samples with the decay product ( $\pi^-$ ) detected. Furthermore, several millions of  $\Xi^-$  events are expected if only the two  $K^+$ 's are detected, sufficient for precise differential cross section measurements. Excited states such as  $\Xi^-(1820)$  can be detected in the reaction of  $\gamma p \rightarrow K^+K^+K^-\pi^-(\pi^-)$ , with the whole decay chain reconstructed, thus enabling the confirmation of its quantum numbers. The expected total number of  $\Xi^-(1820)$  events with the whole decay chain reconstructed would be more than two orders of magnitude higher than what is previously available.

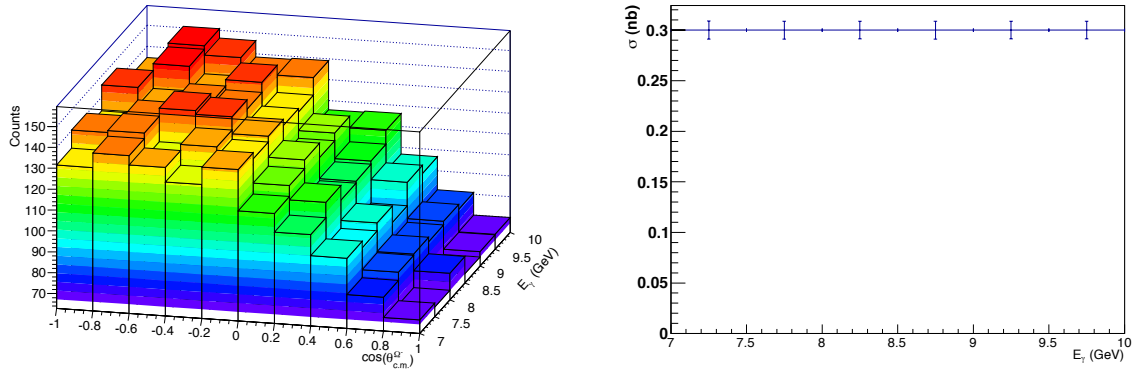


FIG. 27: Projected results for  $\Omega^-$ , reconstructed via the reaction of  $\gamma p \rightarrow K^+ K^+ K^0 (\Omega^-)$ . Left: The expected  $\Omega^-$  counts as a function of  $E_\gamma$  and  $\cos \theta_{c.m.}^{\Omega^-}$ ; Right: Total Cross sections as a function of  $E_\gamma$ .

Therefore, the approved beam time for experiment E12-11-005 would be sufficient to achieve all of our major goals, and no additional beam time would be requested.

- 
- [1] K. Nakamura *et al.* (Particle Data Group), J. Phys. G **37**, 075021 (2010).
- [2] M. Gell-Mann and Y. Ne'eman, *The Eight-fold Way* (W.A. Benjamin, Inc. NY, 1964).
- [3] V.E. Barnes *et al.*, Phys. Rev. Lett. **12**, 204 (1964).
- [4] M. Deuschmann *et al.* (Aachen-Berlin-CERN-Innsbruck-London-Vienna Collaboration), Phys. Lett. **73B**, 96 (1978); M. Baublillier *et al.*, Phys. Lett. **78B**, 342 (1978).
- [5] B. Aubert *et al.* (BaBar Collaboration), Phys. Rev. Lett. **97**, 112001 (2006).
- [6] J.K. Hassall *et al.*, Nucl. Phys. B189, 397 (1981).
- [7] D. Aston *et al.*, Phys. Rev. D **32**, 2270 (1985).
- [8] K. Abe *et al.* (SLAC Hybrid Facility Photon Collaboration), Phys. Rev. D **32**, 2869 (1985).
- [9] S. Capstick and N. Isgur, Phys. Rev. D **34**, 2809 (1986).
- [10] M.I. Adamovich *et al.* (WA89 Collaboration), Eur. Phys. J. C **5**, 621 (1998).
- [11] C. Dionisi *et al.*, Phys. Lett. B **80**, 145 (1978).
- [12] S.F. Biagi *et al.*, Z. Phys. C **9**, 305 (1981).
- [13] S.F. Biagi *et al.*, Z. Phys. C **34**, 15 (1987).
- [14] L. Guo *et al.* (CLAS Collaboration), Phys. Rev. C **76**, 025208 (2007).
- [15] K. Nakayama, Y. Oh, and H. Haberzettl, Phys. Rev. C **74**, 035205 (2006).
- [16] B. Aubert *et al.* (BaBar Collaboration), Phys. Rev. D **78**, 034008 (2008).
- [17] B.M.K. Nefkens, *Baryon spectroscopy and chiral symmetry, Presented at Workshop on 50-GeV Japanese Hadron Facility* (1995).
- [18] A. Duncan, E. Eichten, and H. Thacker, Nucl. Phys. Proc. Suppl. **53**, 299 (1997)
- [19] R. Delbourgo *et al.*, Phys. Rev. D **59**, 113006 (1999).
- [20] V. Fanti *et al.*, Eur. Phys. Rev. D **59**, 113006 (2000).
- [21] R.K. Bradford *et al.* (CLAS Collaboration), Phys. Rev. C **75**, 035205 (2007).
- [22] M.E. McCracken *et al.* (CLAS Collaboration), Phys. Rev. C **81**, 025201 (2010).
- [23] H.J. Lipkin and F. Scheck, Phys. Rev. Lett. **16**, 71 (1966).
- [24] S.V. Bashinsky and R.L. Jaffe, Nucl. Phys. **A625**, 167 (1997).
- [25] S.D. Paganis, T. Udagawa, G.W. Hoffmann, and R.L. Ray, Phys. Rev. C **56**, 570 (1997).
- [26] S.B. Treiman, Phys. Rev. **113**, 355 (1959).
- [27] G.R. Charlton, Phys. Lett. B **32**, 720 (1970).

- [28] R.D.A. Dalmeijer *et al.*, Nuovo Cimento Letters **4**, 373 (1970).
- [29] R.A. Muller, Phys. Lett. **B38**, 123 (1972).
- [30] J.M. Hauptman *et al.*, Nucl. Phys. **B125**, 29 (1977).
- [31] J.K. Ahn *et al.*, Phys. Lett. **B633**, 214 (2006).
- [32] Y. Fujiwara, C. Nakamoto, and Y. Suzuki, Prog. Theor. Phys. **94**, 353 (1995).
- [33] Y. Fujiwara, C. Nakamoto, and Y. Suzuki, Phys. Rev. Lett. **76**, 2242 (1996).
- [34] Y. Fujiwara, C. Nakamoto, and Y. Suzuki, Phys. Rev. C **54**, 2180 (1996).
- [35] C. Nakamoto, Y. Fujiwara, and Y. Suzuki, Nucl. Phys. **A639**, 51c (1998).
- [36] Y. Fujiwara, M. Kohno, C. Nakamoto, and Y. Suzuki, Phys. Rev. C **64**, 054001 (2001).
- [37] W. Roberts and M. Pervin, Int. J. Mod. Phys. A **23**, 2817 (2008); M. Pervin and W. Roberts, Phys. Rev. C **77**, 025202 (2008).
- [38] S. Brodsky, private communication, 2009.
- [39] A. Radyushkin, private communication, 2009.
- [40] J. Badier *et al.* (NA3 Collaboration), Phys. Lett. B **114**, 457 (1982).
- [41] R. Vogt and S.J. Brodsky, Phys. Lett. B **349**, 569 (1995).
- [42] J. K. Shing Man, Yongseok Oh, and K. Nakayama, Phys. Rev. C **83**, 055201 (2011).
- [43] K.-T. Chao, N. Isgur, and G. Karl, Phys. Rev. D **23**, 155 (1981).
- [44] I. Akushevich, H. Bottcher, and D. Ryckbosch, arXiv:hep-ph/9906408.
- [45] M. Dugger, <http://www.public.asu.edu/~dugger/vsGenBriefDescription.pdf>
- [46] S.F. Biagi *et al.*, Z. Phys. C **34**, 175 (1987).
- [47] N. Byers and S. Fenster, Phys. Rev. Lett. **11**, 52 (1963).
- [48] *Meson spectroscopy with low  $Q^2$  electronscattering in CLAS12*, Spokespersons: M. Battaglieri, R. De Vita, D.I. Glazier, C. Salgado, S. Stepanyan, and D. Weygand, JLab Proposal PR-11-005, Newport News, VA, USA, 2011.
- [49] G. Mazzitelli *et al.*, Nucl. Instrum. and Meth. A **515**, 524 (2003).